Journal of Hazardous Materials 514 (2026) 142657

Contents lists available at ScienceDirect

Journal of Hazardous Materials

journal homepage: www.elsevier.com/locate/jhazmat

Environmental forensics of compost-assisted bioremediation in complex co-contaminated soils

Verónica Peña-Álvarez [a,b], Lucía Benavente-Hidalgo [a,c], Eduardo Rodríguez-Valdés [a], Ana I. Peláez [b], José Luis R. Gallego [a,*]

[a] INDUROT and Environmental Biogeochemistry & Raw Materials Group, Campus of Mieres, University of Oviedo, Mieres 33600, Spain
[b] Area of Microbiology, Department of Functional Biology and Environmental Biogeochemistry & Raw Materials Group, Institute of Biotechnology of Asturias (IUBA), Campus of Mieres, University of Oviedo, Mieres 33600, Spain
[c] Biotechnology of Extremophiles Lab, CIQSO-Centro de Investigación en Química Sostenible, I3B and CIDERTA, University of Huelva, Huelva 21007, Spain

HIGHLIGHTS

- Compost amendments markedly enhanced hydrocarbon removal from co-contaminated soil.
- Plant-derived compost outperformed mineral and oleophilic amendments.
- Compost-assisted bioremediation reduced metal-induced constraints on biological activity.
- Integrated chemical and microbial diagnostics explained treatment performance.
- Chemical fingerprinting revealed persistent, non-target organic contaminants.

GRAPHICAL ABSTRACT

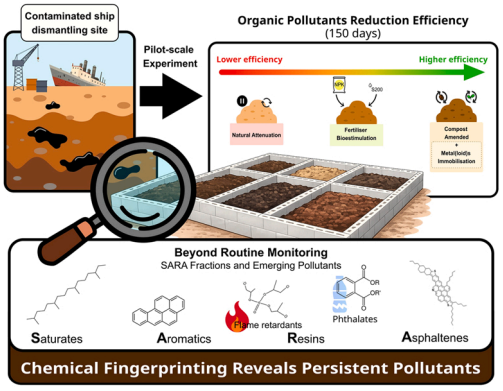

ARTICLE INFO

Keywords:
Bioremediation
Co-contaminated soils
Petroleum hydrocarbons
Microbial community dynamics
Chemical fingerprinting

ABSTRACT

Legacy industrial activities have generated soils co-contaminated with petroleum hydrocarbons, metal(loid)s, and regulated organic pollutants such as polycyclic aromatic hydrocarbons (PAHs) and polychlorinated biphenyls (PCBs). In these complex systems, conventional remediation approaches and concentration-based monitoring often fail to fully capture contaminant transformation processes and residual chemical complexity. Here, pilot-scale field bioremediation was combined with an environmental forensics framework to evaluate contaminant degradation, microbial response, and metal(loid) mobility under realistic field conditions. Six biostimulation strategies were assessed, including plant-derived compost, sludge-based compost, mineral fertilisers, and natural attenuation controls. After 150 days, hydrocarbon removal remained below 30% in control treatments, whereas nutrient-based treatments achieved intermediate efficiencies and compost-amended systems showed the highest performance, reaching up to 58% with plant-derived compost. Compost application was also associated with reductions in TCLP-extractable Zn, Pb, and Cd fractions, consistent with decreased metal mobility. Molecular fingerprinting revealed selective degradation of labile hydrocarbon fractions, while

* Corresponding author.
E-mail address: jgallego@uniovi.es (J.L.R. Gallego).

https://doi.org/10.1016/j.jhazmat.2026.142657
Received 23 March 2026; Received in revised form 8 May 2026; Accepted 8 June 2026
Available online 9 June 2026

biomarkers, asphaltenes, and heavy waxes persisted after treatment. In parallel, non-target screening identified persistent polar contaminants, including organophosphorus flame retardants and phthalates, which were largely unaffected by remediation. Overall, the results demonstrate that compost-assisted bioremediation can enhance hydrocarbon degradation and reduce metal mobility in complex co-contaminated soils, while integrative environmental forensic approaches provide critical insight into residual contaminant complexity not captured by conventional concentration-based metrics.

1. Introduction

Brownfield sites—abandoned or underused industrial areas affected by legacy pollution—pose major environmental and socio-economic challenges due to the persistence, heterogeneity, and complexity of the contaminants present [1,2]. Many of these sites are characterised by long-term, mixed industrial activities that have resulted in the co-occurrence of petroleum hydrocarbons, regulated organic pollutants such as polycyclic aromatic hydrocarbons (PAHs) and polychlorinated biphenyls (PCBs), and metal(loid)s [3–5]. This co-contamination generates complex interactions: while organic contaminants may undergo microbial transformation, metal(loid)s are non-degradable and often exert chronic inhibitory or selective pressures on soil microbial communities [6,7]. These interactions affect contaminant bioavailability, mobility, and toxicity, leading to complex contamination patterns that hinder remediation efforts and delay ecological recovery.

Biological remediation strategies, including biostimulation and compost-assisted bioremediation, are increasingly recognised as sustainable and cost-effective approaches for managing hydrocarbon-contaminated soils [8]. However, their performance in co-contaminated systems remains difficult to predict. Although readily bioavailable hydrocarbons are typically degraded during the early stages, more recalcitrant fractions persist due to ageing processes, sorption to soil particles, and limited bioavailability [9]. Furthermore, the presence of metal(loid)s can exacerbate these limitations by altering redox conditions, enzyme activity, and microbial metabolic pathways. As a result, removal efficiencies observed in simplified or mono-contaminated systems cannot be directly extrapolated to complex field conditions [10]. In response to these challenges, recent research has increasingly focused on integrative and nature-based solutions that combine multiple remediation functions within a single framework [11,12]. Compost amendments, in particular, can enhance hydrocarbon biodegradation while improving soil structure, nutrient availability, and microbial diversity. However, most studies rely primarily on concentration-based metrics (e.g., total petroleum hydrocarbons, TPH), which do not fully capture contaminant transformation processes or the persistence of recalcitrant fractions [13].

To address these limitations, environmental forensics approaches have been increasingly applied to contaminated soils. These approaches combine quantitative analysis with molecular-level diagnostic tools to distinguish between biodegradation and abiotic processes, and to characterise the evolution of different contaminant fractions [9,14]. In particular, gas chromatography–mass spectrometry (GC–MS) fingerprinting and diagnostic ratios provide insights into the selective removal of hydrocarbon compounds and the persistence of resistant biomarkers. In addition, analytical techniques such as pyrolysis–GC–MS (Py–GC–MS) enable the characterisation of complex and highly recalcitrant fractions, including asphaltenes and polymer-associated compounds [15–17]. Beyond regulated contaminants, these approaches can also reveal the presence of non-target or emerging compounds not routinely included in soil monitoring frameworks, such as plastic additives or flame retardants. In this study, these compounds are not treated as primary remediation targets but are considered within a non-target screening framework to assess additional contaminant complexity and to identify potential limitations of conventional monitoring approaches. Their identification provides additional insight into contaminant complexity and may help explain residual environmental constraints and limitations of remediation processes.

Despite growing interest in these integrative approaches, field-scale studies that combine quantitative contaminant analysis, metal mobility assessment, microbial community profiling, and molecular-level fingerprinting remain scarce. Most research has focused on laboratory-scale systems or on single contaminant groups, thereby limiting the transferability of results to real-world conditions. Thus, in this study, we address this gap through a pilot-scale evaluation of bioremediation strategies in a soil co-contaminated with petroleum hydrocarbons (TPH), PAHs, PCBs, and metal(loid)s under field conditions. The specific objectives were to: (i) evaluate the effectiveness of compost-assisted and nutrient-based treatments in enhancing organic pollutants biodegradation and reducing metal bioavailability; and (ii) to demonstrate the added value of an integrated environmental forensics approach for resolving contaminant transformation pathways and identifying overlooked constraints in complex soil systems.

2. Materials and methods

2.1. Study site description

The study was conducted at a former industrial brownfield in Punta Parayas (Camargo, Cantabria, northern Spain), located on the southern margin of the Bay of Santander. Covering approximately 10 ha (Fig. S1a), the site hosted naval ship dismantling activities from the 1960s onwards, which led to the long-term accumulation of petroleum-derived hydrocarbons, PAHs, PCBs, and heavy metal(loid)s. As documented in previous site studies addressing pollutants regulated under the Spanish soil contamination framework (data not shown), this activity resulted in a highly heterogeneous pattern of mixed contamination. The first remediation phase consisted of selective excavation and off-site disposal of the most severely contaminated materials (Fig. S1b). However, subsequent assessments revealed the presence of approximately 30,000 m^3 of residual soil with elevated total petroleum hydrocarbon (TPH, C_{10}–C_{40}) concentrations (Fig. S1b) ranging from 4500 to 10000 $mg \cdot kg^{-1}$, exceeding acceptable risk thresholds defined by a site-specific Quantitative Risk Assessment (QRA). The persistence of this residual contamination, together with the spatial variability of pollutants, justified the implementation of complementary in situ remediation measures. Accordingly, pilot-scale trials were established under field conditions to evaluate compost-assisted and nutrient-based bioremediation strategies.

2.2. Experimental design and bioremediation treatments

Sampling locations were selected based on previous site research and contamination mapping. Excavated soils were subjected to an intensive mixing and homogenisation process to minimise spatial heterogeneity and to obtain a representative bulk material with uniform physicochemical properties. Approximately 12 m^3 of homogenised soil was used to build the experimental units (Fig. S1c), ensuring comparable initial conditions across all treatments.

The pilot-scale bioremediation experiment was conducted under field conditions between April and October of 2024 using six experimental biopiles designed to evaluate natural attenuation and several biostimulation strategies. Each biopile ($2 \times 2 \times 0.5$ m; approximately 2 m^3 of soil) was constructed on a concrete slab to prevent downward

migration of contaminants and leachates. Following homogenisation, the bulk soil was evenly distributed among the six biopiles. Composite samples were collected from each pile at day 0 to verify the uniformity of initial conditions and to characterise baseline physicochemical properties, including petroleum hydrocarbons, PAHs, PCBs, and metals (see Section 3.1).

Six treatment strategies were implemented (Table 1), comprising two natural attenuation controls and four biostimulation approaches. Natural attenuation treatments included a passive control without management (S1) and a managed control subjected to aeration and irrigation only (S2). Biostimulation treatments consisted of the application of a slow-release mineral fertiliser (S3), an oleophilic fertiliser (S4), a sewage sludge–based compost (S5), and a plant-derived compost (S6).

All amendments were applied at the beginning of the experiment and thoroughly mixed into the soil matrix to ensure homogeneous distribution. The slow-release fertiliser (Sierrablen® 31:5:7 N:P:K, Scotts), a granular formulation with a nutrient release period of approximately 2–3 months and previously used in bioremediation contexts [18], was applied at a dose calculated to achieve an optimal C:N ratio of approximately 10:1, following established guidelines for hydrocarbon bioremediation [19]. The second biostimulant tested was S200 (distributed by www.soilutions.es), an oleophilic fertiliser with a C/N/P ratio of 62:5:1 that belongs to a family of oleophilic/lipophilic fertilisers frequently and successfully applied in both marine and terrestrial oil spill cases ([20–22], and references therein). It was applied as a 10% (v/v) aqueous solution by nebulisation in two applications of approximately 100 L each, at the start of the experiment and after 30 days.

The two composts (SC and PC) were supplied by COGERSA (Asturias, Spain). SC was produced from wastewater treatment sludge and shredded wood under forced aeration, while PC was derived from plant residues. Compost amendments were incorporated at a rate of 5% (w/w), followed by moisture adjustment. The main physicochemical characteristics of the two products, together with those of the initial soil, are shown below in Results.

All treatments except the passive control (S1) were regularly irrigated to maintain soil moisture between approximately 60 and 80% of water-holding capacity (corresponding to 15–20% gravimetric moisture). Soil moisture was monitored using a thermobalance and adjusted as required by the addition of distilled and sterilised water (typically 80–100 L per biopile). Aeration was ensured by biweekly mechanical tilling to promote oxygen availability and maintain soil homogeneity.

Table 1
Experimental design and bioremediation treatments applied in the pilot-scale field trial. Fig. S1 shows illustrative images of the procedures followed.

Pile	Treatment Type	Description
S1	Natural Attenuation – Passive	Untreated control exposed to ambient conditions, without irrigation, aeration, or amendments.
S2	Natural Attenuation – Managed	Soil subjected to regular irrigation and mechanical aeration, without nutrient or organic amendments.
S3	Biostimulation – Slow-Release Fertiliser (SRF)	Amended with granular slow-release mineral fertiliser (Sierrablen® 31–5–7 N:P:K) at a dose targeting a C:N ratio of ~10:1, combined with regular irrigation and aeration.
S4	Biostimulation – Oleophilic Fertiliser (S200)	Amended with oleophilic fertiliser (S200) as a 10% (v/v) aqueous solution by nebulisation, applied at day 0 and day 30, with regular irrigation and aeration.
S5	Compost-Assisted Bioremediation with sewage sludge–based compost (SC)	Amended with 5% (w/w) sewage sludge–based compost, combined with regular irrigation and aeration.
S6	Compost-Assisted Bioremediation with plant-based compost (PC)	Amended with 5% (w/w) plant-based compost, with regular aeration and irrigation.

Soil samples were collected from each biopile at six time points: day 0 (baseline), 15, 30, 60, 90, and 150. At each sampling event, composite samples were obtained and analysed for total petroleum hydrocarbons (TPH, C_{10}–C_{40}) and hydrocarbon fractions (see Section 2.4.1). Additional analyses of PAHs, PCBs, metal(loid)s, microbial community structure, and qualitative hydrocarbon fingerprints by GC–MS were performed as described in the following sections. Due to the pilot-scale nature of the experiment, treatments were not replicated at the biopile level. Therefore, the results should be interpreted as system-specific and process-oriented rather than statistically generalisable.

2.3. Physicochemical characterisation of soil and composts

Air-dried initial soil samples, SC and PC were sieved to < 2 mm and homogenised using a roller mill. The > 2 mm fraction was washed and gently abraded to recover adhering fine material, while coarse fragments (gravel and pebbles) were discarded. Representative subsamples of the < 2 mm fraction were obtained by quartering using a channel splitter.

Physicochemical properties were determined following standardised methods. The pH of the soil and amendment was measured in water suspensions (1:2.5, w/v) using a glass electrode, and electrical conductivity was determined in the same extract after dilution (1:5). Total nitrogen was quantified by the Kjeldahl method, available phosphorus by the Olsen method, and organic matter content by loss on ignition (LOI). Particle-size distribution was determined using the Bouyoucos hydrometer method. Total organic carbon (TOC) and inorganic carbon (IC) were measured using a TOC-V CSH analyser (Shimadzu, Japan). Total nitrogen was determined using a LECO CN-200 elemental analyser to support carbon-to-nitrogen (C:N) ratio calculations.

To characterise the elemental composition of soils and organic amendments before treatment, the total concentrations of major and trace elements were determined. Subsamples (0.250 g) were digested by microwave-assisted aqua regia digestion ($HCl:HNO_3$) using a Milestone ETHOS 1 system. Digests were filtered through 0.45 µm membranes, diluted as required, and analysed by inductively coupled plasma mass spectrometry (ICP–MS 7700, Agilent Technologies, USA) using isotopic dilution analysis (IDA) with multi-element spike solutions (ISC Science, Spain).

2.4. Pollutant analysis

2.4.1. TPH quantification

Representative soil samples were sent to an ISO/IEC 17025 certified laboratory (Eurofins Analytico, The Netherlands) to quantify semi-volatile hydrocarbons and obtain partitioning data in terms of carbon chain length (C_{10}-C_{12}, C_{12}–C_{16}, C_{16}–C_{21}, C_{21}–C_{30}, C_{30}–C_{35}, C_{35}-C_{40}) by means of GC-FID (Gas Chromatography-Flame Ionization Detection). Analytical measurements were periodically validated in another accredited laboratory (CIEMSA, Spain).

2.4.2. PAH and PCB congener analysis

For PAH determination, representative 10 g subsamples were extracted with dichloromethane: acetone (1:1) in a Soxtherm apparatus (Gerhardt). The extracts were concentrated by rotary evaporation, and the 16 priority PAHs were measured after injection into a 7890A GC System coupled to a 5975C Inert XL MSD with a Triple-Axis Detector (Agilent Technologies) and following a modification of EPA method 8272. The chromatographic parameters used were as in Baragaño et al. [5]. The mass spectrometer was run in selected ion monitoring (SIM) mode, with quantification based on the following m/z values: 128 (naphthalene); 152, 153, 154 (acenaphthylene and acenaphthene); 165, 166 (fluorene); 178 (phenanthrene and anthracene); 202 (fluoranthene and pyrene); 228 (benz[*a*]anthracene and chrysene); 252 (benzo[*b*]fluoranthene, benzo[*k*]fluoranthene, benzo[*a*]pyrene); and 276, 278

(dibenz[*a*,*h*]anthracene, benzo[ghi]perylene, indeno[1,2,3-cd]pyrene).

PCBs were analysed using the PCB Congener Content Evaluation Revised Mix 1 standard under previously optimised GC–MS configuration [4] and the mass spectrometer in SIM mode. Quantification was performed using the following *m/z* ions: 186, 256, 258 (2,4,4′-trichlorobiphenyl); 220, 290, 292 (2,2′,5,5′-tetrachlorobiphenyl); 256, 326, 328 (2,2′,4,5,5′-pentachlorobiphenyl and 2,3′,4,4′,5-pentachlorobiphenyl); 290, 360, 362 (2,2′,3,4,4′,5′-hexachlorobiphenyl and 2,2′,4,4′,5,5′-hexachlorobiphenyl); and 324, 394, 396 (2,2′,3,4,4′,5,5′-heptachlorobiphenyl). Calibration curves for both PAHs and PCBs were prepared using certified AccuStandard® reference mixtures.

2.4.3. Comprehensive GC–MS and Py–GC–MS study

10-g representative subsamples were extracted with dichloromethane:methanol (3:1, v/v) in a Soxtherm system (Gerhardt, Germany) at 150 °C for 3 h. The extracts were concentrated by rotary evaporation, and aliquots were fractionated and gravimetrically quantified by deasphaltening and liquid chromatography (LC) into four fractions following the SARA (Saturates, Aromatics, Resins and Asphaltenes) procedure [23,24]. SARA fractions are expressed as relative percentages of the extractable organic matter and are interpreted as compositional indicators rather than absolute mass balances. In brief, maltenes and asphaltenes were separated by passing the extracts through 0.45 μm PFTE filters, first using *n*-hexane to remove maltenes, followed by dichloromethane to mobilise asphaltenes. Maltenes were then separated into three fractions according to polarity, from lowest to highest, in an LC column (Corning 7078–5 N serological disposable glass pipette) filled with activated (dried overnight at 240 °C) silica gel (4/5) and alumina (1/5). Saturates (SAT) were eluted with hexane, aromatics (ARO) with dichloromethane:hexane (7:3, v/v), and resins (polars, POL) with dichloromethane:methanol (1:1, v/v). The desaphaltening and LC methodologies are based upon published sources [15]. Blanks, duplicates, and representative standard materials were routinely used for quality control and assurance purposes (QC/QA).

The three maltene fractions were analysed by GC–MS. Extracts were injected into a GCMS-QP2010 Plus (Shimadzu Europe, Germany). A DB-5MS capillary column (5% phenyl, 95% dimethylpolysiloxane; 60 m × 0.25 mm i.d. x 0.1 μm film) from Agilent Tech. was used, with He as carrier gas at 1 mL/min. The initial oven temperature was 50 °C (held for 2 min), which was ramped up at 2.5 °C min^{-1} up to 310 °C and then held for 45 min. The mass spectrometer was operated in EI mode at 70 eV and calibrated daily by auto-tuning with PFTBA. The chromatograms were acquired in full-scan mode (mass range acquisition: 45–500 *m/z*). For quality control, solvent blanks were periodically injected. Compounds were identified using NIST27 and NIST47 mass spectral libraries (https://chemdata.nist.gov/).

Py–GC–MS was performed on a measured representative amount of asphaltene fraction (0.2 mg) for 20 s at 610 °C using a PY-2020iD double-shot pyrolyser (Frontier Lab) connected to the same GC–MS device described above. The oven temperature of the gas chromatograph was programmed from 50 °C to 310 °C (at 2.5 °C min^{-1}), with an initial hold of 2 min at 50 °C and a final hold of 45 min at 310 °C. The mass spectrometer was operated in full-scan mode (50–600 *m/z)*. Pyrolysis products were analysed by GC–MS (Py–GC–MS) using the conditions employed for the other fractions, while the compounds were identified using the aforementioned libraries.

Ratios of compounds were compared to define diagnostic ratios. Selection criteria consisted of abundance in the extract of the initial soil, ease of identification in SIM chromatograms, and representability of the predominant pollutant families. To eliminate the potential varying response of the MS, the ratios were obtained with compounds whose peak areas were measured at the same *m/z* values, as suggested by Kienhuis et al. [25]. Chromatograms with poorly resolved peaks or noisy baselines were discarded.

2.4.4. Heavy metals and metalloids

The concentration of metal(loid)s in soil was determined after digestion with a mixture of nitric and hydrochloric acids in a 1:3 ratio (v:v) in a microwave reaction system (Milestone ETHOS 1, Italy). As, Cd, Cu, Fe, Pb, Zn, and Hg contents were quantified by Inductively Coupled Plasma Mass Spectrometry (ICP-MS 7700; Agilent Technologies, California, USA).

The TCLP test (USEPA method 1311, 1992) was performed to evaluate the potential mobility and availability of heavy metals and metalloids in soil; no additional grinding or disaggregation of the samples was needed as the material was smaller than 1 cm in its narrowest dimension as specified in the method. An acetic acid-based TCLP extraction fluid was prepared with 2.572 g of NaOH and 5.72 mL of glacial acetic acid (pH 4.93 ± 0.05). This test involved stirring 1 g of sample with 20 mL of leaching liquid. After 18 h of mixing, the leachate was passed through a 0.4 μm Millipore filter. The pH of the filtrate was then measured, and the leachate was acidified with a small amount of nitric acid to a pH < 2, followed by ICP-MS analysis. TCLP solution blanks were also measured in order to check the quality of the reagents. TCLP results should be interpreted as an operational measure of potential metal mobility under standardised acidic extraction conditions, enabling comparison among treatments rather than direct prediction of in situ soil behaviour.

2.5. Bacterial community analysis

2.5.1. Culturable heterotrophic bacterial counts

Microbial counting for initial soil and compost was carried out by conventional plate-counting using serial dilutions. To this end, soil and compost serial dilutions were spread on agar plates of Tryptic Soy Broth (Merck, Germany) diluted 1/10 and supplemented with 15% of agar (1/10 TSA). Plates were incubated at 30 °C for 7 days. Cultivable bacteria were then monitored over time in the six microcosms using the same procedure described above.

2.5.2. Bacterial automated ribosomal intergenic spacer analysis

Automated ribosomal intergenic spacer analysis (ARISA) uses the natural length variability of the bacterial 16–23 S rRNA intergenic spacer region to provide a bacterial community profile. ARISA was used to assess changes in bacterial community structure during the microcosm experiments. DNA was extracted with the PowerSoil DNA Isolation Kit (MOBIO Laboratories, Carlsbad, CA, USA) following the manufacturer's instructions. The 16–23 S rRNA intergenic spacer region was amplified using specific ARISA primers, and subsequent fragment analysis was performed as described in Peña-Álvarez et al. [26]. Based on ARISA fragment profiles, β-diversity was determined using a Morisita-Horn dissimilarity matrix, while α-diversity was estimated with Hill numbers, and group differences were evaluated with the non-parametric analysis of similarities (ANOSIM).

3. Results and discussion

3.1. Characterisation of initial soil and amendments

The initial characterisation highlighted marked contrasts between the contaminated soil and the two organic amendments selected for detailed physicochemical analysis (i.e., composts; Table 2). The slow-release mineral fertiliser (SRF) and the oleophilic fertiliser (S200) were applied following the manufacturer's specifications and previous bioremediation studies and were therefore not subjected to independent physicochemical characterisation.

The soil had an alkaline pH (8.2) and relatively high electrical conductivity, reflecting its industrial legacy and the presence of soluble salts. Nutrient availability was extremely limited, particularly nitrogen (0.03%) and available phosphorus (3 mg·kg^{-1}), resulting in an unfavourable nutrient balance for microbial activity and clearly supporting the need for biostimulation. In contrast, the two composts showed near-

Table 2
Initial physicochemical properties and contaminant concentrations of the soil and organic amendments used in the field bioremediation trials (values correspond to the <2 mm fraction). Parameters include pH, electrical conductivity, nutrients, carbon forms, major and trace elements, and organic contaminants (TPH, PAHs, and PCBs), and they were used to define baseline conditions prior to treatment application. Relative standard deviations (RSD) were below 5% for all parameters, except for TPH (<11%), PAHs (<9%), and PCBs (<10%).

Parameters		Units	Soil	SC	PC	*Reference values/thresholds*
Physico-chemical parameters	pH		8.2	7.3	7.5	6–7[(1)]
	Conductivity	µS/cm	1840	1313	1171	< 2000[(2)]
	Nitrogen	%	0.03	2.55	2.3	> 1.5[(2)]
	Phosphorus (available)	mg/kg	3	406	306	7–18[(1)]
Carbon	TOC	%	2.79	26.63	24.20	> 1.2[(1)]
	IC		0.97	0.77	0.77	-
Major elements	Fe	%	0.6	3.6	1.1	2.5[(3)]
	Al		0.7	1.4	1.0	5.8[(3)]
	K		0.1	1.0	1.9	1.6[(3)]
	Na		0.1	3.4	2.2	0.6[(3)]
	Ca		3.1	6.4	5.6	0.7[(3)]
	Mg		0.6	0.7	0.7	0.5[(3)]
Trace elements	Cu	$mg \cdot kg^{-1}$	1566	172	46	4000[(3)]
	Zn		4100	685	260	10,000[(3)]
	As		58.5	14.2	7.5	200[(3)]
	Cd		7.7	1.6	1.0	200[(3)]
	Pb		1767	90	33	800[(3)]
Organics	TPH (C_{10}-C_{40})	$mg \cdot kg^{-1}$	6050	4250	790	50[(4)]
	PAH		59.88	10.11	2.06	
	PCB		0.97	0.10	0.12	0.8[(4)]

[(1)] European Environment Agency (2023), Soil monitoring in Europe-Indicator and thresholds for soil health assessment. https://www.eea.europa.eu/en/analysis/publications/soil-monitoring-in-europe
[(2)] Hazelton PA (2016) Interpreting Soil Test Results. https://doi.org/10.1071/9781486303977
[(3)] EuroGeoSurveys (EGS) (2006). FOREGS Geochemical Atlas of Europe. http://weppi.gtk.fi/publ/foregsatlas/
[(4)] BOPA 91 21-IV-2014 (2014). Niveles Genéricos de Referencia para metales pesados en Suelos del Principado de Asturias. https://medioambiente.asturias.es/documents/646140/0/ASTURIAS-RESOLUCION-20-03-2014-NGR.pdf/
[(5)] Real Decreto 9/2005 (2005). Actividades potencialmente contaminantes del suelo y los criterios y estándares para la declaración de suelos contaminados. https://www.boe.es/boe/dias/2005/01/18/pdfs/A01833-01843.pdf

neutral pH values and substantially higher nutrient contents, especially nitrogen and available phosphorus, confirming their suitability as organic amendments. TOC contents in the composts were approximately one order of magnitude higher than in the soil, indicating a strong potential to stimulate microbial growth and improve soil structure, while inorganic carbon contents were comparable across materials, suggesting a similar contribution from carbonate phases.

In terms of major elements, the soil was characterised by elevated Ca concentrations and moderate Fe and Al contents, consistent with local geochemical background conditions and historical anthropogenic inputs. The composts showed higher concentrations of Fe, K, Na, and Ca, reflecting their organic origin and the incorporation of mineral fractions during the composting process. In turn, trace element analysis revealed markedly elevated concentrations of Cu, Zn, and Pb in the soil, well above typical background levels (Table 2). In contrast, both composts exhibited substantially lower trace metal concentrations, minimising the risk of introducing additional metal loads during amendment application.

Organic contaminant analysis confirmed the heavily impacted nature of the soil, with high concentrations of TPH, together with detectable levels of PAHs and PCBs. Although both composts contained residual hydrocarbons and trace amounts of PAHs and PCBs, their concentrations were one order of magnitude lower than those measured in the soil, indicating that compost application did not represent a significant additional source of organic contamination.

Overall, these results emphasise the severe nutrient limitation and multi-contaminant character of the soil, while highlighting the complementary role of organic composts in supplying carbon, nutrients, and buffering capacity. Of note, as shown in Table 2, the initial concentrations of several organic and inorganic pollutants clearly exceeded the reference values established under current Spanish soil legislation, thus justifying the implementation of risk-based remediation strategies at this site.

3.2. General evolution of bioremediation treatments

3.2.1. Temporal dynamics of TPH

Fig. 1 shows the temporal evolution of TPH (C_{10}–C_{40}) under the different bioremediation strategies tested over the 150-day pilot trial. Initial TPH concentrations were comparable across all treatments (≈5500–6500 $mg \cdot kg^{-1}$ dry weight), confirming homogeneous starting conditions and allowing a robust comparison of treatment performance.

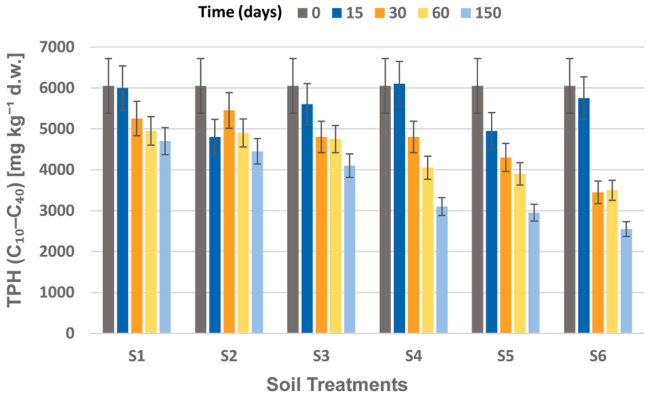

Fig. 1. Temporal evolution of total petroleum hydrocarbons (TPH, C_{10}–C_{40}) in soils subjected to different bioremediation treatments over 150 days. Error bars represent the relative variability associated with measurements of composite samples taken in the same biopile (n = 6) and reflect the progressive homogenisation of the system over time under field conditions. Due to the pilot-scale design (one biopile per treatment), statistical comparisons between treatments should be interpreted with caution. Observed trends are supported by complementary evidence from PAH removal and chemical fingerprinting analyses. *Treatments: S1, natural attenuation (static); S2, natural attenuation with irrigation and tilling (dynamic); S3, slow-release fertiliser (SRF); S4, oleophilic fertiliser (S-200); S5, SC; S6, PC.*

Natural attenuation treatments showed limited remediation efficiency. The passive control (S1) exhibited only marginal TPH reductions throughout the monitoring period, while the managed control (S2), involving irrigation and periodic tilling but no nutrient or organic amendment, achieved slightly higher removal. This behaviour is consistent with a landfarming-type effect driven by improved aeration and moisture control, but it also highlights the intrinsic limitations of unassisted biodegradation in nutrient-depleted, co-contaminated soils [27]. Consistently, all biostimulation strategies enhanced hydrocarbon removal relative to natural attenuation. Both the slow-release mineral fertiliser (S3) and the oleophilic fertiliser (S4) induced an initial rapid decrease in TPH concentrations during the first 60 days, followed by a markedly slower removal phase. This two-stage pattern suggests early stimulation of microbial activity, which was subsequently constrained by nutrient depletion, contaminant ageing, or limited bioavailability of the remaining hydrocarbon fractions.

Compost-assisted treatments yielded the highest remediation efficiencies. The sewage sludge-based compost (SC, S5 cell) promoted a sustained and progressive decline in TPH concentrations throughout the trial, whereas the plant-derived compost (PC, S6 cell) consistently outperformed all other treatments, reaching the lowest residual TPH levels at day 150. Overall, TPH removal efficiencies remained below 30% in the control treatments (S1 and S2), reached 32% in S3 and 49% in S4, and increased to 51% and 58% in the compost-amended systems S5 and S6, respectively.

Taken together, these results demonstrate that compost-assisted bioremediation substantially enhances hydrocarbon removal compared to both natural attenuation and mineral-based biostimulation under field conditions, as previously reported [8,9]. The superior performance of plant-derived compost (S6) points to a more favourable combination of nutrient supply, organic carbon availability, and microbial stimulation.

3.2.2. Hydrocarbon fractions

Changes in the distribution of TPH fractions by carbon number provide additional insight into the degradation processes operating under the different treatments. Also, GC–FID-based fractionation supports most regulatory frameworks and site-specific risk assessment procedures applied to contaminated soils.

Relative to the initial soil, all treatments showed a pronounced depletion of the lighter hydrocarbon fractions (C_{10}-C_{12} and C_{12}–C_{16}), consistent with the preferential biodegradation of more labile compounds and, to a lesser extent, volatilisation processes, as widely reported in the literature ([9] and references therein). These compositional changes were most evident in treatments achieving higher overall TPH removal, particularly in compost-amended systems. Across all treatments, the intermediate fraction (C_{21}–C_{30}) remained dominant throughout the experiment. In contrast, heavier fractions (C_{30}–C_{35} and C_{35}–C_{40}) became progressively enriched in relative terms as biodegradation advanced, reflecting the increasing recalcitrance and reduced bioavailability of the residual hydrocarbon pool [8].

Natural attenuation treatments retained a comparatively higher proportion of intermediate fractions, indicating limited progression beyond early-stage degradation. Conversely, compost-amended biopiles—especially the PC treatment (S6; Fig. S2)—displayed more advanced degradation patterns, characterised by substantial depletion of bioavailable fractions and relative enrichment of heavier hydrocarbons. These trends are consistent with enhanced microbial activity and more effective transformation of labile hydrocarbons under compost-assisted bioremediation.

3.2.3. Bacterial counts

The temporal evolution of culturable heterotrophic microbial populations during the pilot trial is shown in Fig. S3. Initial microbial abundances were comparable across all treatments (approximately 8.2–8.4 log CFU·g^{-1} dry soil), thereby indicating similar biological starting conditions following soil homogenisation.

Natural attenuation treatments (S1 and S2) showed limited microbial growth stimulation throughout the experiment, as reflected by heterotrophic bacteria counts. In the static control (S1), microbial counts remained relatively stable or declined slightly over time, whereas the dynamically managed control (S2) exhibited greater temporal variability and a marked decrease toward the end of the trial. This behaviour likely reflects progressive nutrient depletion and sustained stress associated with persistent contamination. In contrast, all biostimulation treatments induced a clear, albeit transient, increase in bacterial counts during the early and intermediate phases of the experiment. Compost-amended biopiles (S5 and S6) showed the strongest response, reaching peak values between 30 and 60 days (>9.0 log CFU·g^{-1}), consistent with enhanced nutrient availability, organic carbon input, and improved soil conditions, as well as the direct introduction of microorganisms [28]. This initial stimulation was followed by a gradual decline, potentially linked to substrate depletion and the progressive removal of readily biodegradable hydrocarbons [29].

Of note, the PC treatment (S6) maintained higher microbial abundances at 150 days compared to all other treatments, in agreement with its superior TPH removal efficiency. This sustained microbial activity suggests the development of a functionally robust and resilient community capable of withstanding co-contaminant stress under field conditions.

3.3. Fate of PAHs and PCBs

Table 3 summarises the concentrations of PAHs and PCBs after 150 days of treatment. PAHs are grouped by molecular weight (2–3, 4, and 5–6 rings) and PCBs by the number of Cl atoms.

As shown above, initial total PAH concentrations were approximately 60 mg kg^{-1}, with a predominance of 4-ring compounds, followed by 5–6 and 2–3 ring PAHs. After 150 days, natural attenuation treatments (S1 and S2) showed only marginal reductions in total PAHs, confirming the limited effectiveness of unassisted biodegradation under co-contaminated conditions. Biostimulation treatments led to more substantial PAH removal, particularly for low- and medium-molecular-weight compounds. The most pronounced decreases were observed in the compost-amended biopiles, especially S6 (plant-based compost), where total PAHs were reduced by more than 50% relative to initial levels. This reduction was driven mainly by the depletion of PAHs containing 2–3 and 4 rings, which are generally more bioavailable and susceptible to microbial degradation. Sludge compost (S5) and the slow-release fertiliser treatment (S3) also led to notable decreases in total PAHs, although to a lesser extent. In contrast, high-molecular-weight PAHs (5–6 rings) showed greater persistence across treatments [19], and in some cases an apparent relative enrichment, particularly under natural attenuation [18].

As regards PCBs, initial total concentrations were close to 1 mg kg^{-1} and were dominated by penta- and hexachlorinated congeners, reflecting the historical industrial origin of contamination and the intrinsic persistence of higher-chlorinated PCBs in soil matrices. After 150 days, all treatments showed some degree of PCB reduction; however, marked differences in efficiency and congener profiles were observed between remediation strategies. Natural attenuation treatments (S1 and S2) resulted in only moderate decreases in total PCB concentrations, with limited removal of highly chlorinated congeners. In contrast, biostimulation treatments enhanced PCB attenuation, particularly for lower- and mid-chlorinated congeners (3–5 Cl). Compost-amended biopiles showed the highest removal efficiencies, with the PC treatment (S6) achieving the lowest residual total PCB concentration (0.22 mg kg^{-1}), followed by SC (S5) and the slow-release fertiliser treatment (S3). Hexa- and heptachlorinated PCBs (6–7 Cl) were the most persistent congeners across all treatments, consistent with their strong hydrophobicity, low bioavailability, and high resistance to aerobic biodegradation. These properties limit the desorption of these

Table 3
PAH and PCB content (mg·kg^{-1} d.w.) in initial soil and after 150-day field-trial experiments under the different conditions tested. *Treatments: S1, natural attenuation (static); S2, natural attenuation with irrigation and tilling (dynamic); S3, slow-release fertiliser (SRF); S4, oleophilic fertiliser (S-200); S5, sludge-based compost; S6, plant-derived compost. 2-ring PAHs (naphthalene); 3-ring PAHs (fluorene + acenaphthylene + acenaphthene + phenanthrene + anthracene); 4-ring PAHs (fluoranthene + pyrene + benz[a]anthracene + chrysene); 5–6 ring PAHs (benzo[b]fluoranthene + benzo[k]fluoranthene + benzo[a]pyrene + dibenz[a,h]anthracene + benzo[ghi]perylene + indeno[1,2,3-cd]pyrene). PCB molecule ranges are labelled with 'n Cl', which represents the set of isomers with 'n' chlorine atoms. Relative Standard Deviations (RSD) for individual PAHs ranged from 1% for benzo(a)anthracene to 9% for naphthalene, and below 10% for all PCB families.*

				After 150 days					
			Initial	S1	S2	S3	S4	S5	S6
PAH	**2–3 rings**	mg kg^{-1}	13.13	10.31	10.45	7.06	9.95	8.17	4.88
	4 rings		29.27	25.42	23.47	18.96	21.35	18.17	13.34
	5–6 rings		17.48	23.21	20.6	17.52	17.95	16.28	10.29
	∑ PAH		59.88	58.93	54.52	43.53	49.26	42.63	28.51
PCB	**3–4 Cl**		0.12	0.02	0	0.02	0.03	0.02	0
	5 Cl		0.29	0.08	0.06	0.05	0.1	0.05	0.03
	6 Cl		0.43	0.2	0.19	0.16	0.26	0.15	0.11
	7 Cl		0.13	0.11	0.13	0.1	0.15	0.09	0.07
	∑ PCB		0.97	0.42	0.37	0.33	0.53	0.31	0.22

contaminants from soil particles and reduce microbial accessibility, resulting in slow degradation rates compared with less-chlorinated congeners [30,31]. Nevertheless, a progressive decrease in these highly chlorinated fractions was observed in compost-amended systems, suggesting that enhanced microbial activity and improved physicochemical conditions may indirectly promote their attenuation. Organic amendments can increase contaminant bioavailability through changes in sorption–desorption equilibria, stimulation of co-metabolic pathways, and enhancement of microbial community diversity and enzymatic potential, thereby facilitating the transformation of otherwise recalcitrant PCB congeners [32,33].

Overall, the results for PAHs and PCBs are consistent with the TPH data, reinforcing that compost-assisted bioremediation—especially with PC—promotes advanced degradation stages. However, the remaining levels found are probably a limiting factor as the process achieved a relevant reduction of total PAH and PCB burdens, and altered ring/congener distributions, but did not attain complete or quasi-complete degradation.

3.4. Metal availability and interaction with bioremediation

Total metal(loid) concentrations confirmed the highly contaminated nature of the soil, particularly with respect to Zn, Cu, and Pb, which were present at levels typical of long-term industrial activities. As expected, total contents remained unchanged throughout the pilot trial and therefore only initial values are reported as a reference context (Table 4). In contrast, pronounced differences were observed in the TCLP-extractable fractions after 150 days, highlighting the influence of the different treatments on metal bioavailability rather than on total metal loads.

Natural attenuation treatments (S1 and S2) showed limited or inconsistent effects on metal mobility. In several cases, TCLP-extractable concentrations were comparable to or higher than initial values, particularly for Cu and Zn. These findings thus suggest that aeration and moisture control alone were insufficient to promote metal immobilisation and may even enhance this process through organic matter degradation or changes in soil redox conditions. Similarly, biostimulation using slow-release fertiliser (S3) and the oleophilic amendment (S4) did not systematically reduce metal bioavailability, i.e., nutrient addition without organic matter inputs does not effectively mitigate metal mobility.

In contrast, compost-amended treatments (S5 and S6) led to a marked reduction in the bioavailable fractions of most metals. The most pronounced decreases were observed for Zn and Pb, whose TCLP-extractable concentrations were reduced by approximately 60–65% with SC (S5) and PC (S6) treatments compared to initial values. Cd was fully immobilised to below detection limits in both compost-amended soils, while Ni also showed a clear reduction, particularly in the PC treatment (S6). Cu bioavailability decreased more moderately but still followed the same overall trend. In turn, As remained below detection limits in TCLP extracts across all treatments, indicating limited mobility under the prevailing soil conditions and confirming that this metalloid did not act as a bioavailability-driven constraint during the bioremediation process.

The observed compost-induced reductions in metal bioavailability reflect well-documented stabilisation mechanisms, including enhanced organic matter complexation and sorption processes, which reduce contaminant accessibility. These changes are consistent with a decrease in inhibitory constraints on microbial activity and may contribute to the enhanced degradation trends observed [34–36], thereby indicating that compost amendments not only promote the biodegradation of organic pollutants but also reduce the bioavailability of several potentially toxic metal(loid)s. This dual functionality is particularly relevant in co-contaminated soils, where metal toxicity can limit microbial activity

Table 4
Total metal concentrations and TCLP-extractable fractions in the soil before treatment and after 150 days under the different bioremediation strategies. Total concentrations (mg·kg^{-1} d.w.) correspond to initial soil characterisation. TCLP-extractable concentrations (mg·kg^{-1}) are shown for the initial soil and for each treatment at the end of the pilot trial on day 150. *Treatments: S1, natural attenuation (static); S2, natural attenuation with irrigation and tilling (dynamic); S3, slow-release fertiliser (SRF); S4, oleophilic fertiliser (S-200); S5, SC; S6, PC. Values marked with an asterisk indicate statistically significant differences compared to the initial TCLP-extractable concentration (* $p < 0.05$). Given the pilot-scale nature of the experiment, results are discussed mainly in terms of relative trends among treatments.*

Element	Total (mg·kg^{-1})	TCLP initial (mg·kg^{-1})	TCLP after 150 days (mg·kg^{-1})					
			S1	S2	S3	S4	S5	S6
Ni	158	2.5	1.8	1.7	2.1	1.6	1.1*	0.4*
Cu	1566	3.2	6.3	6.7	8.2	6.3	5.3*	3.1*
Zn	4100	150.0	154.1	132.6	182.6	123.2	53.7*	59.9*
As	58.5	0.0	0.0	0.0	0.0	0.0	0.0	0.0
Cd	7.7	0.6	0.7	0.8	0.6	0.7	0.0	0.0
Pb	1767	2.4	2.9	2.4	2.5	2.7	0.6*	1.4*

and compromise bioremediation efficiency. The stronger immobilisation observed with plant-derived compost is consistent with its higher organic carbon content and its superior performance in hydrocarbon removal, reinforcing its suitability as a multifunctional amendment for sustainable remediation strategies.

3.5. Microbial community structure (ARISA)

Bacterial dynamics along the experiment were evaluated through ARISA fingerprinting. Although ARISA does not provide taxonomic resolution, microbial fingerprinting approaches have proven useful for the rapid, inexpensive, and reliable assessment of microbial community dynamics [37,38]. Fig. 2 summarises the ARISA results, including beta-diversity through NMDS ordination based on the Morisita-Horn dissimilarity matrix (Fig. 2a) and alpha-diversity estimated using Hill numbers: richness (q0) and evenness (E2.0) scatter plot (Fig. 2b), as well as Hill numbers of order q = 1 (Fig. 2c) and q = 2 (Fig. 2d).

NMDS ordination of ARISA profiles (Fig. 2a) revealed clear

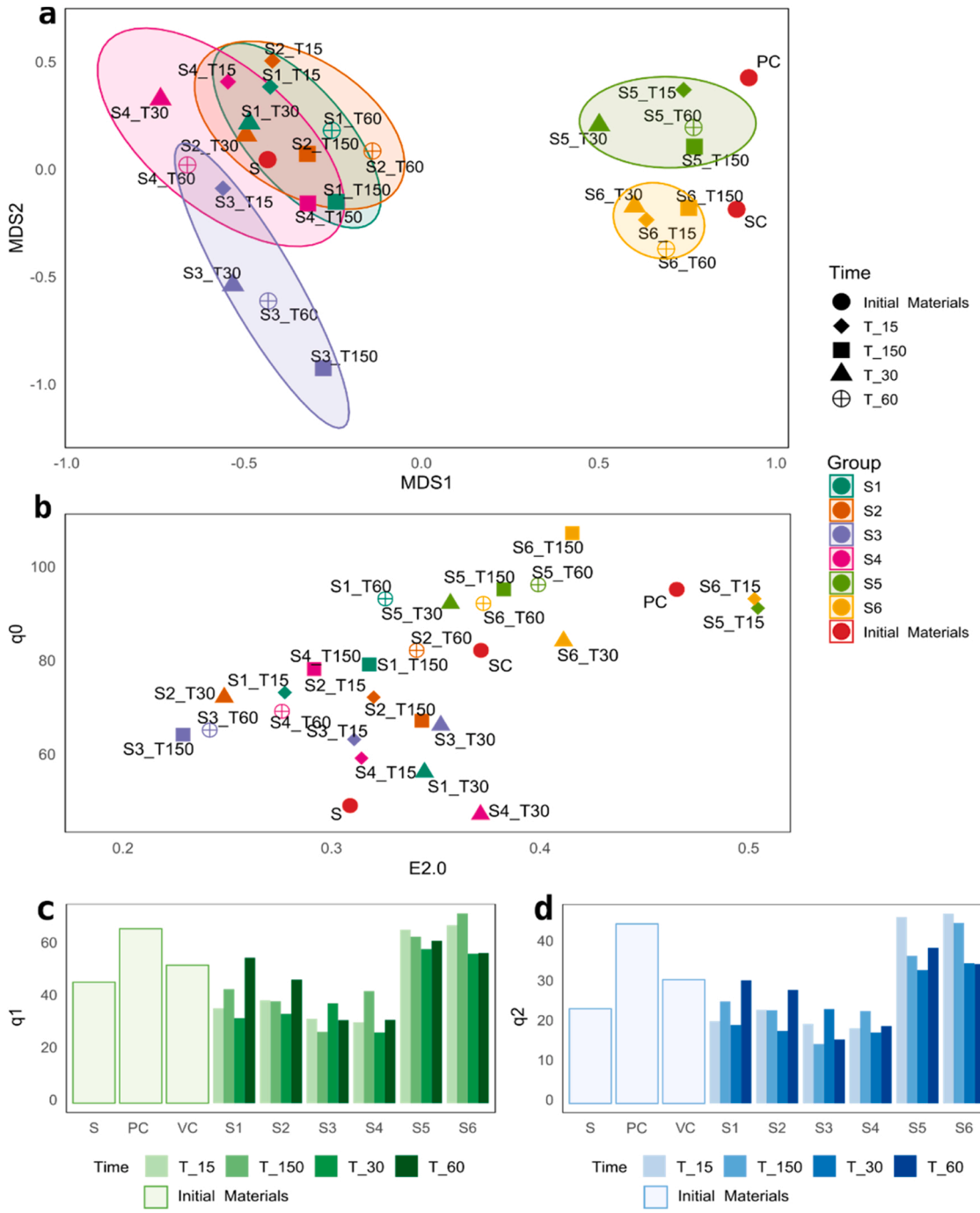

Fig. 2. Diversity and community structure metrics derived from ARISA (Automated Ribosomal Intergenic Spacer Analysis) bacterial fingerprinting profiles. (a) Non-metric multidimensional scaling (NMDS) ordination showing similarities among bacterial community structures across treatments and sampling times (Shepard plot non-metric fit = 0.984). NMDS axes represent relative ecological distances among samples, and ellipses enclose 70% of the observations for each treatment group. (b) Richness-evenness scatter plot illustrating relationships between bacterial community richness and distribution uniformity. (c, d) Hill diversity numbers of order $q = 1$ and $q = 2$, representing diversity metrics increasingly weighted toward dominant taxa. *Treatments: S1, natural attenuation (static); S2, natural attenuation with irrigation and tilling (dynamic); S3, slow-release fertiliser (SRF); S4, oleophilic fertiliser (S-200); S5, sludge-based compost; S6, plant-derived compost.*

clustering patterns grouped by remediation strategies, which was supported by the ANOSIM test. Treatment strategy had a significant effect on community composition ($R = 0.6981$, $p = 0.0001$), whereas experiment time had a limited effect on bacterial community shift ($R = 0.1037$, $p = 0.0855$).

Natural attenuation treatments (S1 and S2) clustered closely and showed minimal temporal displacement in the NMDS plot, consistent with their modest TPH removal capacity, limited PAH and PCB attenuation, and negligible effects on metal bioavailability. Alpha-diversity metrics in S1 and S2 were generally low, including richness, evenness, and Hill numbers $q = 1$ and $q = 2$, and remained similar to the initial soil. Taken together, these results indicate that natural attenuation, under both static and dynamic conditions, had no relevant impact on bacterial community structure, in line with the limited hydrocarbon removal observed.

Fertilisation treatments showed divergent patterns. S4 (oleophilic fertiliser) remained closer to the controls S1 and S2 in the NMDS plot, whereas SRF addition (S3) caused a shift in beta-diversity, diverging from both the control and the initial soil community. However, this structural shift was not accompanied by increased alpha-diversity metrics, suggesting a compositional rearrangement rather than diversification. A plausible interpretation is that water-soluble nutrient addition (N and P) removed key ecological constraints, thereby altering selective pressures. Microbial groups specialised in nitrogen fixation or phosphorus solubilisation, formerly advantageous under nutrient-limited conditions, may have been outcompeted by faster-growing taxa, leading to community reorganisation without increased diversity [39–41]. Furthermore, despite reducing nutrient limitations, the lack of bioavailable carbon and the recalcitrant nature of the contaminants likely prevented significant enhancement of hydrocarbon degradation in S3 [42,43]. In addition, in some cases, excess nitrogen added to polluted soils can reduce hydrocarbon remediation rates by disrupting microbial symbioses and weakening bacteria-fungal interactions [44], thereby redefining microbial community functional capacities [45]. However, this shift was not observed in S200 fertilised soil (S4), likely due to capacity of the formulation of S200 to improve hydrocarbon bioavailability by delivering nutrients in the oil phase [46,47], thereby enhancing hydrocarbon-degrading microorganisms [46,48] already present in the initial soil. This decoupling between community change and functional outcome highlights the importance of pollutant bioavailability and substrate quality in biostimulation strategies.

In contrast, compost-amended treatments (S5 and S6) showed pronounced and persistent divergence from all other treatments, with limited temporal drift, indicating early and strong restructuring of the bacterial community. consistent with the introduction and establishment of compost microbial community [49,50]. However, compost-amended soil communities also separated from each other in the NMDS ordination, suggesting that composts of different origins imprint distinct microbial signatures [51]. Compost amendments also produced the highest and most sustained alpha-diversity values, particularly under the plant-derived compost. These observations are consistent with the assembly of more complex and functionally diverse communities capable of addressing mixed pollution: in petroleum-contaminated soils, compost increases bacterial/fungal α-diversity and enhances TPH and PAH removal [9,28], while in metal-impacted soils, compost elevates microbial diversity and activity [52].

Overall, these results align with remediation performance: S6 showed the highest capacity to remove pollutants, followed by S5, whereas S1 and S2 showed the poorest performance. Taken together, the ARISA results support the notion that compost-assisted bioremediation not only enhances hydrocarbon removal but also promotes microbial community configurations associated with broader contaminant attenuation, including organic pollutants and metal bioavailability. Functionally, compost can enrich hydrocarbon-degrading gene pools [53] and, through organic-matter inputs, contribute to reduced metal bioavailability [54,55], both of which are relevant under co-contamination scenarios. It should be noted that ARISA provides a fingerprint of community structure but does not offer taxonomic resolution or functional gene information. Future studies integrating high-throughput sequencing approaches (e.g., 16S rRNA amplicon sequencing or metagenomics) would allow a more detailed understanding of the relationships between microbial community composition, functional potential, and contaminant degradation processes.

3.6. Chemical fingerprinting and environmental forensics

Our analytical approach combines quantitative target analysis (e.g., TPH, PAHs, PCBs), aligned with regulatory frameworks, with compositional and non-target screening techniques aimed at resolving contaminant transformation pathways and identifying overlooked compounds. Therefore, based on the overall performance of the different treatments, a detailed chemical fingerprinting analysis was conducted on selected representative systems—namely the initial soil, the natural attenuation control (S1), and the plant-based compost–amended biopile (S6)—to gain mechanistic insight into contaminant transformation pathways and to identify compounds not captured by routine regulatory monitoring. This targeted approach allowed deeper exploration of the processes underlying the contrasting remediation efficiencies observed among treatments.

Prior to GC–MS analyses, separation of organic matter into fractions on the basis of polarity using SARA fractionation (saturates, aromatics, resins, and asphaltenes) was used to assess the fate of both labile and recalcitrant hydrocarbon pools, with particular emphasis on the evolution of heavy fractions (Table 5).

The overall trends were initially consistent with previous studies on biodegradation of hydrocarbon-contaminated soils [9,23,56]: Both saturate and aromatic fractions showed substantial depletion over time, reflecting preferential biodegradation of more bioavailable hydrocarbons. In contrast, a relative enrichment of polar compounds (resins) and, more markedly, asphaltenes was observed, particularly in the compost-amended treatment. This pattern reflects the progressive concentration of recalcitrant fractions as biodegradation advances and highlights the need for detailed molecular-level analysis beyond bulk hydrocarbon metrics.

Accordingly, a detailed characterisation of each SARA fraction was subsequently performed to elucidate transformation pathways and assess the extent of degradation within traditionally considered recalcitrant hydrocarbon pools.

3.6.1. Saturate fraction

The chemical fingerprint of the saturate fraction is shown in Fig. 3, comparing the initial soil with samples collected after 150 days of treatment with the natural attenuation control (S1) and the biopile amended with plant-derived compost (S6). The total ion chromatograms (TIC; Fig. 3, left panels) revealed a broad distribution of compounds dominated by alkanes, spanning from low- to very high-molecular-weight hydrocarbons, including compounds with more than 40 carbon

Table 5
Relative composition (%) of the four SARA fractions (saturates, aromatics, resins, and asphaltenes) in the initial soil, S1 and S6 biopiles after bioremediation. Changes in SARA composition were used to assess selective hydrocarbon degradation and the persistence of recalcitrant petroleum fractions during treatment. Results represent the average of three analytical determinations, with relative standard deviations (RSD) below 5%.

Sample	SARA fractions (%)			
	SATURATES	AROMATICS	POLAR	ASPHALTENE
Initial	38	30	19	13
S1 after 150 days	25	24	25	26
S6 after 150 days	21	23	21	35

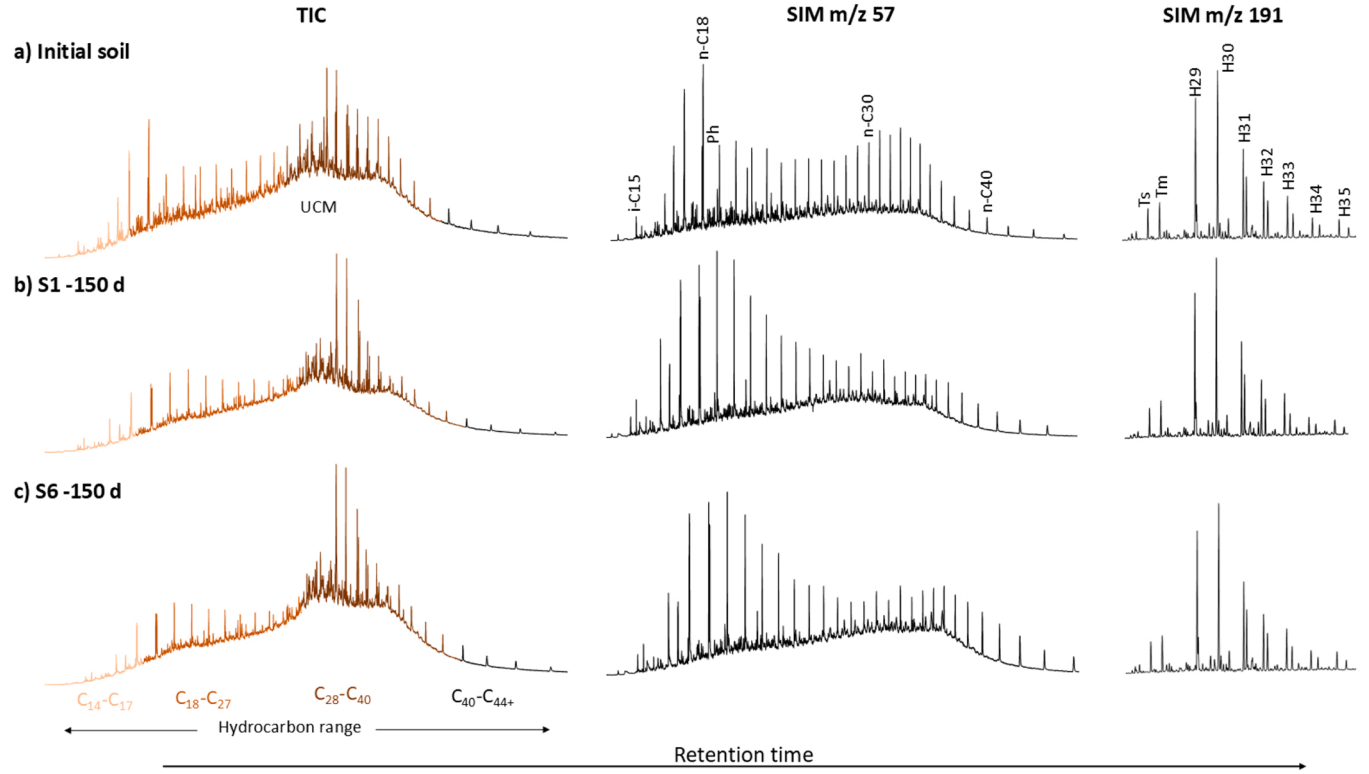

Fig. 3. Gas chromatographic fingerprints of the saturate fraction obtained in TIC mode (left panels), SIM mode at *m/z* 57 (middle panels), and SIM mode at *m/z* 191 (right panels) for: (a) the initial soil, (b) the natural attenuation control after 150 days (S1), and (c) the biopile amended with plant-derived compost after 150 days (S6). Chromatograms illustrate the distribution of n-alkanes (C_{13} to $>C_{40}$), isoprenoids, hopanes, and the unresolved complex mixture (UCM), highlighting compositional changes associated with biodegradation processes. Abbreviations: n-Cn, linear alkanes; Ph, phytane; H29, C29 17α(H),21β(H)-30-norhopane; H30, C30 17α(H),21β(H)-hopane; H31–H35, homohopane series; Ts, 18α(H),21β(H)-22,29,30-trisnorneohopane; Tm, 17α(H),21β(H)-22,29,30-trisnorhopane.

atoms. This wide-ranging alkane profile is typical of heavy fuel oil, commonly associated with maritime activities, such as those used in cargo ships and large vessels [57].

The initial chromatograms (Fig. 3a) already showed a pronounced unresolved complex mixture (UCM), indicative of prior biodegradation and weathering processes. After 150 days of treatment, the UCM signal became more prominent, particularly in the PC-amended soil (Fig. 3c), reflecting further selective removal of more labile hydrocarbons and enrichment of recalcitrant components. In turn, selected ion monitoring (SIM) chromatograms targeting *m/z* 57 (Fig. 3, middle panel), a fragment diagnostic of alkanes, revealed abundant *n*-alkanes ranging from n-C_{15} to n-C_{44}, together with isoprenoids such as i-C_{15}, pristane, and phytane. In addition, hopanes (C_{29}–C_{35}), detected at *m/z* 191 (Fig. 3, right panel), were consistently present across all samples.

Comparison of pre- and post-treatment profiles showed a progressive depletion of light and mid-range *n*-alkanes (C_{13}–C_{27}) and enhancement of the UCM hump, indicating advanced biodegradation of labile saturates, in agreement with the quantitative TPH and chain-fractionation results presented above. In contrast, the hopane series exhibited no discernible changes in either relative abundance or distribution after treatment, confirming their high resistance to biodegradation and supporting their use as conserved molecular markers of petroleum origin, as the most recalcitrant constituents within the saturate fraction [14,15]. The persistence of high-molecular-weight compounds (C_{28}–C_{40}) reflects their increased recalcitrance and reduced bioavailability in aged petroleum residues [58].

To further evaluate the relative contribution of biodegradation and volatilisation processes affecting the saturate fraction, several diagnostic alkane ratios were calculated (Table 6). These indices are commonly used to track the preferential removal of *n*-alkanes relative to more recalcitrant isoprenoids and to identify potential evaporation effects [56,59].

The *n*-C_{18}/phytane ratio showed a marked decrease after 150 days, particularly in S6, and to a lesser extent in the natural attenuation control (S1). This trend reflects the well-established preferential biodegradation of linear alkanes relative to branched isoprenoids and is consistent with the chromatographic evidence discussed above. A similar behaviour was observed for medium- to high-molecular-weight *n*-alkanes, as indicated by the decline in the *n*-C_{30}/phytane ratio, further supporting the occurrence of biologically driven transformation processes. In contrast, the *n*-C_{40}/phytane ratio did not show a consistent decreasing trend and even exhibited a slight increase in S6. This lack of a

Table 6
Evolution of selected diagnostic ratios used to assess biodegradation and volatilisation effects within the saturate fraction after 150 days of treatment, calculated from SIM (Single Ion Mode) chromatograms (*m/z* = 57). Percentage change is expressed relative to initial values.

Samples	i-C_{15}/Ph		n-C_{18}/Ph		n-C_{30}/Ph		n-C_{40}/Ph	
	Ratio	% Change	Ratio	% Change	Ratio	% Change	Ratio	% Change
Initial	0.05	0.00	1.56	0.00	0.27	0.00	0.29	0.00
S1 150 days	0.02	53.50	0.88	43.81	0.17	36.67	0.24	15.07
S6 150 days	0.01	85.91	0.71	54.27	0.14	48.15	0.31	−7.64

clear response suggests limited biodegradation of very heavy waxy alkanes, likely due to their reduced bioavailability and strong association with the solid phase, as previously reported for aged petroleum residues [15,46].

The isoprenoid ratio *i*-C_{15}/phytane also decreased substantially in both S1 and, more prominently, in S6, indicating that branched alkanes were also affected by transformation processes. Given the relatively small differences in volatility between *i*-C_{15} and phytane [56], this decrease is attributed primarily to biodegradation, although a minor contribution from volatilisation could not be completely ruled out. Evaporation played a negligible role in saturate fraction evolution, as GC fingerprints showed no truncation or enrichment patterns, and the lightest detectable compounds remained in the C_{13}–C_{14} range. Since GC retention time correlates with vapour pressure, this confirms that biodegradation, rather than volatilisation, was the dominant process [60].

3.6.2. Aromatic fraction

The aromatic fraction of the initial soil (Fig. 4a) presented a highly complex composition covering a wide molecular weight range. As shown in the total ion chromatograms (left panel of Fig. 4), the dominant compounds corresponded to PAHs and, to a lesser extent, PCBs, which had been previously quantified in Section 3.3. The distribution was characterised by the predominance of 4- and 5-ring PAHs, together with the presence of very high-molecular-weight compounds containing up to seven aromatic rings, such as coronene, further confirming the heavy and highly weathered nature of the contaminant mixture, in agreement with the evidence derived from the saturate fraction. In addition to parent PAHs, the initial fingerprint showed a strong contribution of alkylated homologues, particularly alkyl-PAHs (right panel of Fig. 4) and alkylbenzenes (middle panel), which are typical markers of petroleum-derived inputs [15,59]. Sulphur-containing heterocyclic compounds, mainly alkyl-dibenzothiophenes ($m/z = 212$; not shown), were also detected, consistent with contamination by heavy fuel oils, commonly characterised by notable S contents [15].

Bioremediation led to a marked simplification of the aromatic fingerprints, reflected in both a reduction in compound diversity and a decrease in signal intensity. These changes were evident in the natural attenuation control (Fig. 4b) and became much more pronounced in the compost-amended biopile (Fig. 4c). The most marked effect was observed for alkylated aromatic compounds, particularly alkylbenzenes and alkyl-PAHs, which were preferentially depleted relative to their parent PAHs. This shift is clearly illustrated in the merged SIM chromatograms of alkylphenanthrenes (Fig. 4, right panel), where methyl-, dimethyl-, and trimethyl-substituted phenanthrenes became progressively less abundant than compared to the parent compound. These detailed SIM profiles further reveal that biodegradation was not uniform within compound families, as certain isomers were selectively removed faster than others, highlighting the strong structural control on biodegradation kinetics. Aromatic biomarkers, such as triaromatic steroids (detected at $m/z = 231$), were also identified (not shown). They revealed negligible variation across treatments, behaving analogously to hopanes in the saturate fraction, and confirming their suitability as conservative internal markers of weathering and biodegradation ([9, 61], and references therein).

Overall, the evolution of the aromatic fraction corroborates that compost-assisted bioremediation promotes advanced biodegradation stages, preferentially targeting alkylated and more bioavailable aromatic compounds while leaving behind a residue dominated by highly condensed and recalcitrant structures.

3.6.3. Polar fraction

The polar fraction, which accounted for approximately 20% or more of the extractable organic matter in all samples, provided particularly

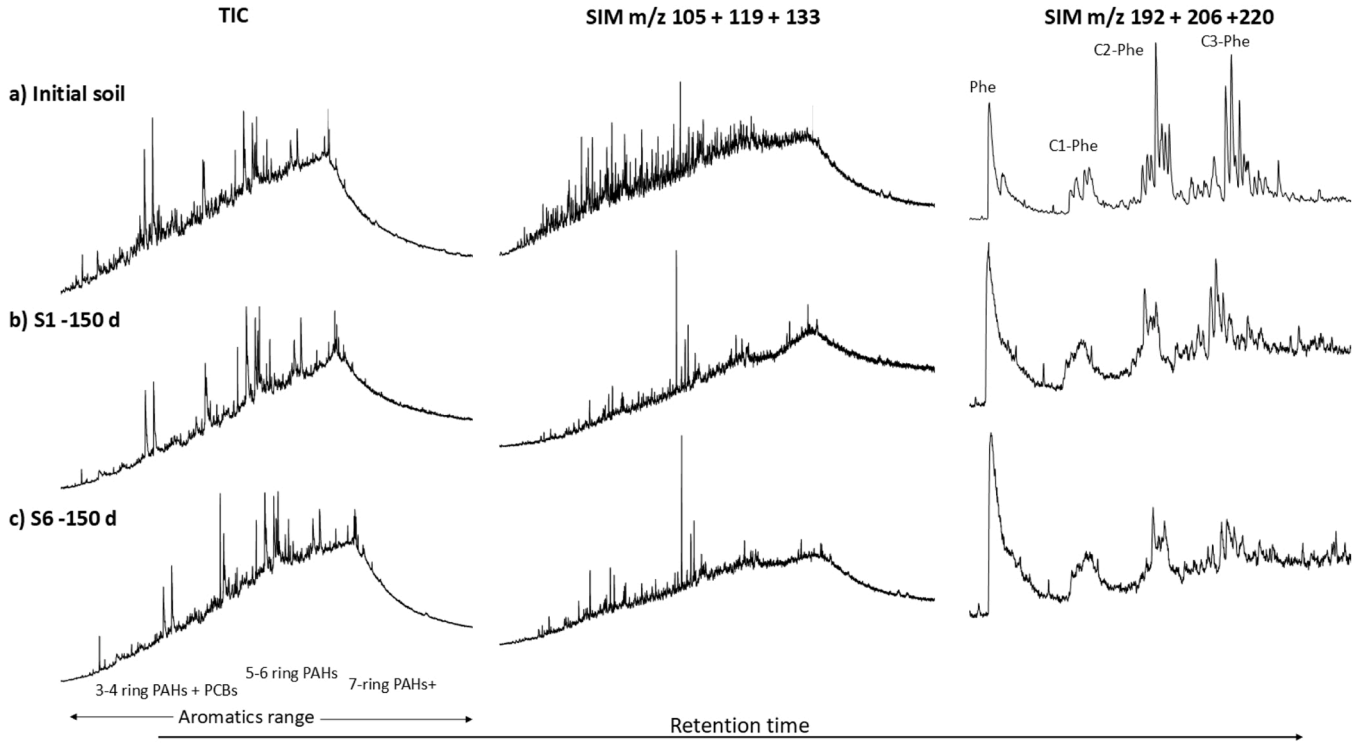

Fig. 4. Aromatic hydrocarbon fingerprints obtained by GC–MS for: (a) the initial soil, (b) the natural attenuation control after 150 days (S1), and (c) the biopile amended with plant-derived compost after 150 days (S6). Left panels: representative total ion chromatograms (TIC). Middle panels: merged SIM chromatograms of alkylbenzenes (m/z 105 + 119 + 133). Right panels: merged SIM chromatograms of alkylphenanthrenes (m/z 192 + 206 + 220). Chromatograms reveal the preferential depletion of alkylated aromatic compounds and selective isomer degradation after treatment, particularly in the compost-amended system. Abbreviations: Phe, phenanthrene; C1-Phe, methylphenanthrenes; C2-Phe, dimethylphenanthrenes; C3-Phe, trimethylphenanthrenes.

relevant insights into the complexity of the contamination and the limitations of conventional remediation assessments. It was analysed using a non-target screening approach; therefore, results are qualitative and intended to identify compound classes and persistence patterns rather than to provide absolute quantification. The GC–MS data (Fig. 5) revealed several classes of compounds undetected by routine regulatory analyses and not currently included in soil quality legislation.

As shown in the total ion chromatograms (left panel of Fig. 5), three main families dominated the polar fraction: organophosphorus flame retardants, phthalates, and plant-derived sterols (including Freidelin), while there is no clear evidence of the presence of brominated flame retardants.

The organophosphorus compounds shown in the central panel are widely used as flame retardants and are increasingly recognised for their toxicity, environmental persistence, and potential to affect soil and biota in a similar manner to other emerging contaminants, including brominated flame retardants [62,63]. The main component of this group is tris (2-chloroisopropyl) phosphate (TCIPP), which accounts for approximately 50–85% of commercial chlorinated phosphate flame-retardant mixtures and has been extensively used in a variety of formulations for rigid and flexible polyurethane foams and other polymeric materials as a replacement for banned or restricted brominated products [64]. Given the relevance of TCIPP and its apparent absence from soils under the specific trade names considered here [63], its molecular structure is shown in Fig. S4, together with the diagnostic mass spectrum used for its unequivocal identification. The remaining compounds in this group are structural isomers of TCIPP with much lower abundances in the mixture. Their chromatographic profiles remained essentially unchanged across treatments, indicating a marked recalcitrance to biodegradation under the conditions tested and suggesting that these organophosphate esters can persist even in biologically active systems [62]. Although detailed ecotoxicological evaluation lies beyond the scope of the present study, the persistence and toxicity of these isomers of TCIPP point to a potential contribution to residual soil toxicity and to selective pressures on microbial communities, with possible implications for soil health, nutrient cycling, and the long-term success of bioremediation.

Phthalates, clearly identified in the right panel of Fig. 5, were also abundant in all samples, indicating the presence of plasticisers and plastic-derived materials and suggesting the likely occurrence of micro- and nanoplastics within the soil matrix [65]. Only after 150 days were minor changes in their relative abundance observed, even in the compost-amended biopile. These observations are consistent with previous reports describing phthalate esters and co-occurring plastic debris as poorly biodegradable and prone to persistence in terrestrial systems [66]. In contrast, the third group of polar compounds consisted mainly of plant sterols and structurally related biogenic markers, which are common constituents of natural soils and are frequently used as indicators of higher-plant inputs and organic matter turnover [67,68]. As expected, these compounds were markedly enriched in the PC-amended biopile (Fig. 5c), reflecting the additional plant-derived organic matter supplied with the amendment rather than the persistence of anthropogenic contaminants.

The detection of organophosphorus flame retardants (e.g., TCIPP) and phthalates is consistent with the industrial context of the study site, where ship dismantling activities involve a wide range of materials such as plastics, insulation foams, coatings, and electrical components. These compounds are commonly used as additives in such materials, and their presence reflects the multi-source and heterogeneous nature of contamination in brownfield environments. Their co-occurrence with petroleum hydrocarbons is therefore more likely related to overlapping

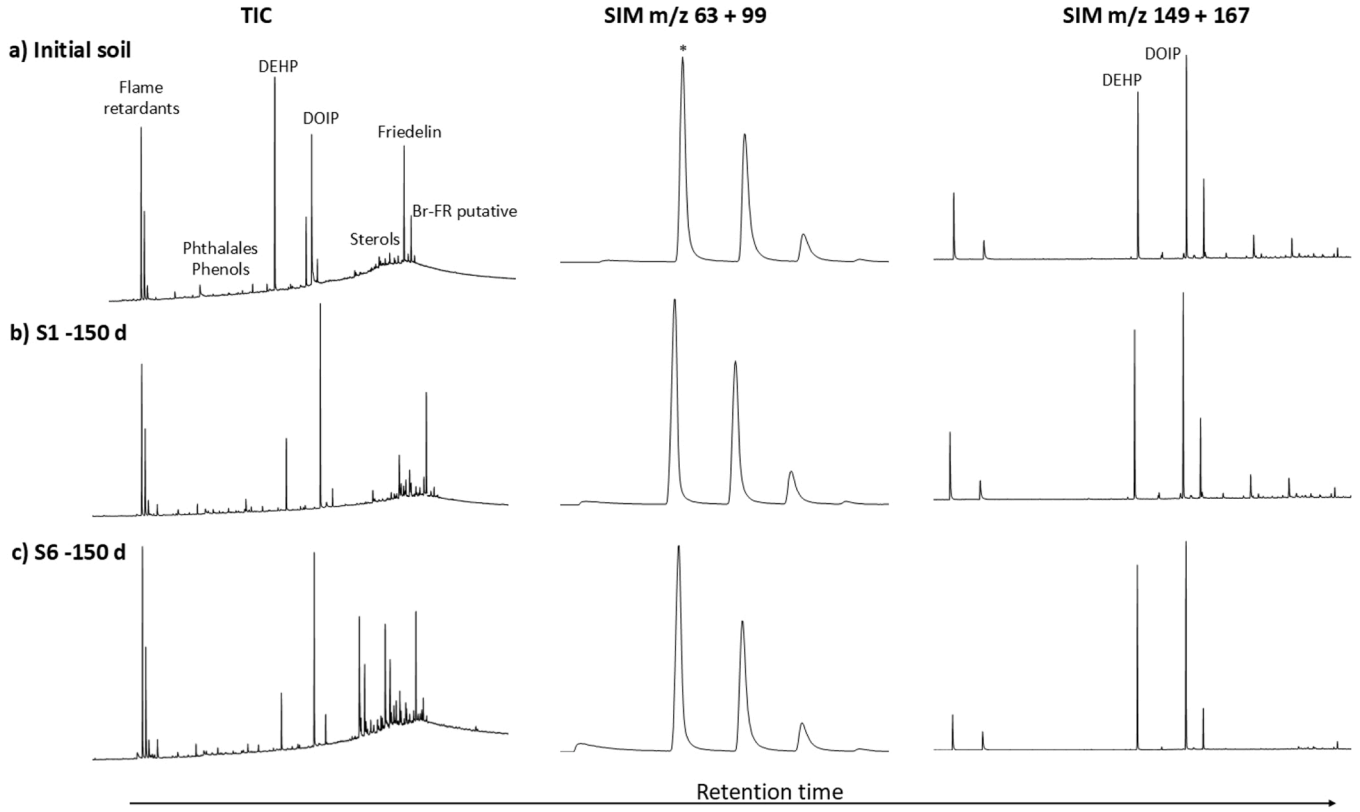

Fig. 5. Polar compound fingerprints obtained by GC–MS for: (a) the initial soil, (b) the natural attenuation control after 150 days (S1), and (c) the biopile amended with plant-derived compost after 150 days (S6). Left panels: representative total ion chromatograms (TIC). Middle panels: merged SIM chromatograms of chlorinated organophosphorus flame retardants (m/z 63 + 99). Right panels: merged SIM chromatograms of phthalates (m/z 149 + 167). Chromatograms reveal the persistence of several polar contaminants following treatment, including flame retardants and phthalates. Abbreviations: DEHP, bis(2-ethylhexyl) phthalate; DOIP, dioctyl isophthalate; Br-FR, putative brominated flame retardants; *, tris(2-chloroisopropyl) phosphate (TCIPP).

contamination sources than to shared transformation pathways.

These findings underscore the intrinsic limitations of bioremediation when dealing with highly recalcitrant polar compounds and emphasise that even highly effective and versatile amendments such as compost may not fully address all contaminant classes in complex co-contaminated soils, reinforcing the need for integrative risk assessment frameworks that go beyond conventional target analytes.

3.6.4. *Asphaltene fraction*

As shown above in Table 5, the relative contribution of the asphaltene fraction increased with the degree of biodegradation of the contaminant mixture, reflecting the preferential removal of more labile saturate and aromatic compounds and the concomitant enrichment of the most recalcitrant, high-molecular-weight components [69]. This trend should therefore not be interpreted as evidence of extensive asphaltene degradation, but rather as indicative that the bioremediation processes in this system are largely controlled by the selective depletion of more accessible hydrocarbon fractions. Given their structural complexity, high degree of aromatic condensation, and very high molecular weight, asphaltenes are generally considered poorly biodegradable under typical soil bioremediation conditions, and they often serve as a long-term, refractory reservoir of organic matter in heavily weathered residues [70]. Accordingly, the pyrochromatograms shown in Fig. 6 are dominated by thermal decomposition products derived from highly condensed aromatic and aliphatic structures, which are characteristic of asphaltene matrices and consistent with previous applications of analytical Py–GC–MS to weathered petroleum residues [71,72].

Despite this overall recalcitrance, the presence of very long-chain *n*-alkanes in the asphaltene pyrolysates is noteworthy. These compounds correspond to the high–molecular-weight aliphatics previously observed in the saturate fraction and are particularly pronounced in the PC-amended biopile (Fig. 6c). These findings suggest that compost addition introduced plant-derived polymers whose transformation and partial fermentation promoted the formation or preservation of long-chain aliphatic residues within the asphaltene pool. Therefore, the behaviour of the asphaltene fraction in this study confirms its role as a terminal reservoir for the most refractory organic compounds in heavily contaminated soils. Furthermore, it illustrates how bioremediation can indirectly reshape contaminant composition through selective degradation of more labile fractions rather than through direct transformation of these ultra-heavy components.

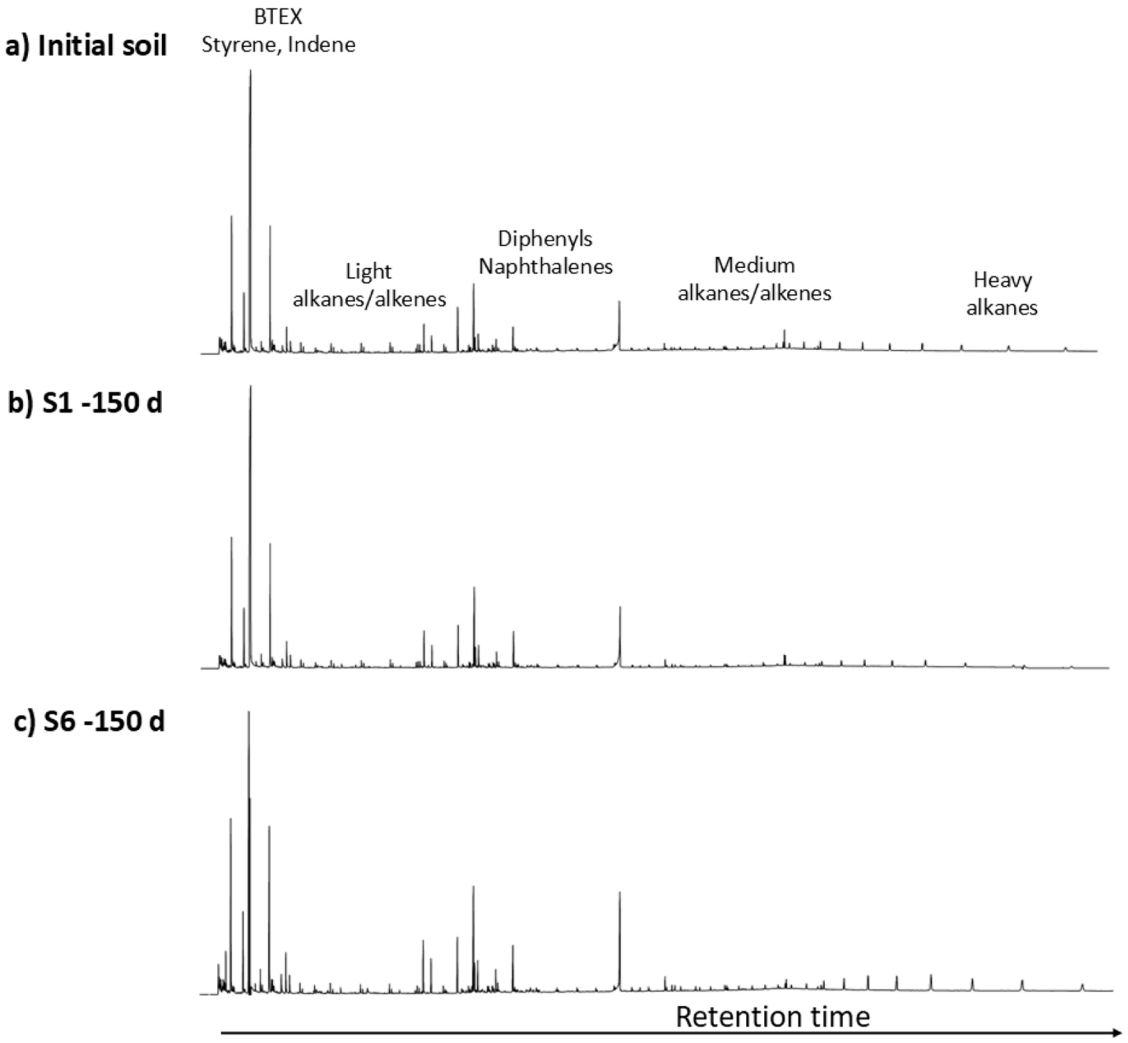

Fig. 6. Full-scan pyrochromatographic fingerprints of the asphaltene fraction for: (a) the initial soil, (b) the natural attenuation control after 150 days (S1), and (c) the biopile amended with plant-derived compost after 150 days (S6). Pyrograms are dominated by thermal decomposition products derived from highly condensed aromatic and aliphatic structures characteristic of asphaltenes. The persistence of these complex fractions after treatment highlights the recalcitrant nature of residual hydrocarbon pools, while the increased contribution of long-chain *n*-alkanes in the compost-amended system suggests selective enrichment of resistant aliphatic compounds during biodegradation.

3.7. Integrated overview of contaminant dynamics and microbial response

The combined evaluation of contaminant concentrations, molecular fingerprints, bacterial community structure, and metal mobility indicates that treatment performance was governed by interconnected processes involving contaminant bioavailability, microbial adaptation, and selective transformation pathways. Rather than evolving independently, these components followed coupled trajectories in which changes in one domain influenced the others. Although replication at the biopile scale was not feasible under pilot-scale conditions, the consistency observed across complementary analytical approaches supports the robustness of the identified process trends. Under field conditions, differentiation between biotic and abiotic processes was addressed through diagnostic ratios and molecular fingerprinting approaches rather than sterilized controls, which are neither feasible nor environmentally representative at this scale.

Bioremediation resulted in a clear reduction of petroleum-derived hydrocarbons, particularly in the treatment amended with plant-derived compost. However, qualitative analyses demonstrated that hydrocarbon removal was highly fraction- and compound-specific, reflecting selective biodegradation processes controlled by substrate accessibility and microbial capability. The superior performance of plant-derived compost is consistent with the combined effects of several complementary mechanisms. Its higher content of labile organic matter likely stimulated microbial activity and supported the development of hydrocarbon-degrading communities, while improvements in soil structure and aeration may have enhanced oxygen availability and favoured aerobic degradation pathways. At the same time, the observed reduction in metal bioavailability suggests that compost amendment contributed to the immobilisation of metal(loid)s, thereby reducing metal-related constraints on microbial metabolism. Together, these coupled effects provide a mechanistic framework consistent with the enhanced hydrocarbon removal, microbial community shifts, and reduced metal mobility observed in this treatment.

The preferential depletion of low- and medium-molecular-weight alkanes and alkylated aromatics coincided with marked shifts in bacterial community structure, as evidenced by ARISA profiles and diversity metrics. These patterns suggest a progressive selection of microbial consortia capable of exploiting increasingly complex substrates, indicating feedback between substrate availability and community composition. The transition from labile hydrocarbons toward more recalcitrant pools, including biomarkers and asphaltenes, reflects the sequential nature of biodegradation processes. Likewise, the persistence of hopanes, triaromatic steroids, and heavy waxes further supports the interpretation that biodegradation, rather than physical losses, dominated contaminant evolution.

Metal dynamics followed a partially decoupled yet interacting pathway. While total metal concentrations remained largely unchanged, TCLP-extractable fractions decreased over time, particularly in compost-amended treatments, indicating reduced mobility and potential toxicity. TCLP results should be interpreted as an operational measure of potential metal mobility under standardised acidic extraction conditions, enabling comparison among treatments rather than direct prediction of in situ soil behaviour. The observed decrease in extractable metal fractions was consistent with the concurrent increase in organic matter complexity and polar fractions, which can promote metal immobilisation through sorption and complexation processes. In turn, reduced metal bioavailability may have alleviated inhibitory effects on microbial activity, consistent with the enhanced hydrocarbon degradation trends observed.

Non-target screening of polar and asphaltene fractions added a critical dimension to the assessment by revealing contaminant groups not captured by conventional monitoring metrics. The persistence of flame retardants and phthalates, which were largely unaffected by treatment, contrasted with the dynamic transformation of hydrocarbons and highlighted a decoupling between bulk contaminant removal and residual chemical complexity. These observations suggest that improvements in traditional indicators such as TPH reduction may not fully reflect changes in overall soil chemical composition or potential environmental relevance. Although no quantitative risk assessment was performed, the co-occurrence of advanced hydrocarbon biodegradation with persistent emerging contaminants highlights potential implications for residual risk and reinforces the need for integrative assessment frameworks, including approaches based on Py–GC–MS fingerprinting [73,74].

4. Conclusions

This pilot-scale field study demonstrated that compost-assisted bioremediation can effectively enhance hydrocarbon degradation and reduce metal mobility in complex co-contaminated soils. Among the evaluated treatments, plant-derived compost showed the best overall performance, achieving the highest TPH removal efficiencies together with pronounced shifts in microbial community structure and reduced TCLP-extractable metal fractions.

Molecular fingerprinting revealed that hydrocarbon removal was highly selective, with preferential depletion of labile and moderately recalcitrant compounds, while more resistant fractions such as hopanes, asphaltenes, and heavy waxes persisted after treatment. In parallel, non-target GC–MS and Py–GC–MS analyses identified persistent polar contaminants, including organophosphorus flame retardants and phthalates, which were largely unaffected by remediation.

The combined results demonstrate that remediation performance in co-contaminated soils is governed not only by bulk contaminant removal, but also by changes in contaminant bioavailability, molecular composition, and microbial adaptation. In this context, the integration of quantitative analyses, molecular fingerprinting, microbial indicators, and metal mobility assessment provided complementary process-level information that could not be captured by conventional concentration-based metrics alone.

Overall, this study highlights the value of integrative environmental forensic approaches for improving the assessment of remediation processes and identifying residual contaminant complexity under realistic field conditions.

Environmental Implication

This work demonstrates that remediation of co-contaminated soils requires assessment approaches that go beyond bulk contaminant concentrations to better capture contaminant transformation and residual chemical complexity. Compost-assisted bioremediation proved effective for enhancing hydrocarbon degradation while reducing metal mobility. In parallel, molecular fingerprinting approaches revealed persistent and non-target contaminants not identified by conventional monitoring. These findings highlight the value of integrating advanced chemical diagnostics and bioavailability-oriented metrics into site-specific remediation assessment and long-term environmental management.

CRediT authorship contribution statement

Verónica Peña-Álvarez: Writing – original draft, Visualization, Methodology, Investigation, Conceptualization. **Gallego Jose Luis R.:** Writing – original draft, Visualization, Supervision, Project administration, Methodology, Investigation, Funding acquisition, Conceptualization. **Peláez Ana Isabel:** Writing – review & editing, Supervision, Methodology. **Rodriguez-Valdés Eduardo:** Resources, Methodology, Data curation. **Lucía Benavente-Hidalgo:** Methodology, Investigation, Formal analysis, Data curation, Conceptualization.

Declaration of Competing Interest

The authors declare that they have no known competing financial

interests or personal relationships that could have appeared to influence the work reported in this paper.

Acknowledgements and funding

This work was supported by INTERSOIL project (PID2023-147718NB-I00, AEI/Spain, FEDER/EU) and SEKUENS funding (SEK-25-GRU-GIC-24-043, Asturias, Spain). We gratefully acknowledge the support of Rymoil S.A., which supplied samples, civil works and partial funding. We would like also to thank the Environmental Assay Unit of the Scientific and Technical Services of the University of Oviedo for technical support.

Appendix A. Supporting information

Supplementary data associated with this article can be found in the online version at doi:10.1016/j.jhazmat.2026.142657.

Data availability

Data will be made available on request.

References

[1] O'Connor, D., Zheng, X., Hou, D., Shen, Z., Li, G., Miao, G., et al., 2019. Phytoremediation: climate change resilience and sustainability assessment at a coastal brownfield redevelopment. Environ Int 130, 104945. https://doi.org/10.1016/j.envint.2019.104945.

[2] Pizzol, L., Critto, A., Agostini, P., Marcomini, A., 2011. Regional risk assessment for contaminated sites. Part 2: ranking of potentially contaminated sites. Environ Int 37 (8), 1307–1320. https://doi.org/10.1016/j.envint.2011.05.010.

[3] Díaz, A.M., Baragaño, D., Menéndez-Aguado, J.M., Norén, A., Karlfeldt Fedje, K., Espín, E., et al., 2025. Enhanced remediation of organotin compounds and metal (loid)s in polluted sediments: chemical stabilization with mining-wastes and nZVI versus physical soil washing. J Environ Manag 373, 123602. https://doi.org/10.1016/j.jenvman.2024.123602.

[4] Fernández, B., Lara, L.M., Menéndez-Aguado, J.M., Ayala, J., García-González, N., Salgado, L., et al., 2020. A multi-faceted, environmental forensic characterization of a paradigmatic brownfield polluted by hazardous waste containing Hg, As, PAHs and dioxins. Sci Total Environ 726, 138546. https://doi.org/10.1016/j.scitotenv.2020.138546.

[5] Baragaño, D., Ratié, G., Sierra, C., Chrastný, V., Komárek, M., Gallego, J.R., 2022. Multiple pollution sources unravelled by environmental forensics techniques and multivariate statistics. J Hazard Mater 424, 127413. https://doi.org/10.1016/j.jhazmat.2021.127413.

[6] Xu, Y., Seshadri, B., Bolan, N., Sarkar, B., Ok, Y.S., Zhang, W., et al., 2019. Microbial functional diversity and carbon use feedback in soils as affected by heavy metals. Environ Int 125, 478–488. https://doi.org/10.1016/j.envint.2019.01.071.

[7] Zeng, K., Huang, X., Guo, J., Dai, C., He, C., Chen, H., et al., 2024. Microbial-driven mechanisms for the effects of heavy metals on soil organic carbon storage: a global analysis. Environ Int 184, 108467. https://doi.org/10.1016/j.envint.2024.108467.

[8] Curiel-Alegre, S., Velasco-Arroyo, B., Rumbo, C., Khan, A.H.A., Tamayo-Ramos, J. A., Rad, C., et al., 2022. Evaluation of biostimulation, bioaugmentation, and organic amendments application on the bioremediation of recalcitrant hydrocarbons of soil. Chemosphere 307, 135638. https://doi.org/10.1016/j.chemosphere.2022.135638.

[9] Gallego, J.L.R., Peña-Álvarez, V., Lara, L.M., Baragaño, D., Forján, R., Colina, A., et al., 2022. Effective bioremediation of soil from the Burgan oil field (Kuwait) using compost: a comprehensive hydrocarbon and DNA fingerprinting study. Ecotoxicol Environ Saf 247, 114267. https://doi.org/10.1016/j.ecoenv.2022.114267.

[10] Zhang, X., Zhang, X., Wang, S., Zhao, S., 2022. Improved remediation of co-contaminated soils by heavy metals and PAHs with biosurfactant-enhanced soil washing. Sci Rep 12 (1), 3801. https://doi.org/10.1038/s41598-022-07577-7.

[11] Lee, H., Sam, K., Coulon, F., De Gisi, S., Notarnicola, M., Labianca, C., 2024. Recent developments and prospects of sustainable remediation treatments for major contaminants in soil: a review. Sci Total Environ 912, 168769. https://doi.org/10.1016/j.scitotenv.2023.168769.

[12] Romantschuk, M., Lahti-Leikas, K., Kontro, M., Galitskaya, P., Talvenmäki, H., Simpanen, S., et al., 2023. Bioremediation of contaminated soil and groundwater by in situ biostimulation. Front Microbiol 14, 1258148. https://doi.org/10.3389/fmicb.2023.1258148.

[13] Leech, C., Tighe, M.K., Pereg, L., Winter, G., McMillan, M., Esmaeili, A., et al., 2020. Bioaccessibility constrains the co-composting bioremediation of field aged PAH contaminated soils. Int Biodeterior Biodegrad 149, 104922. https://doi.org/10.1016/j.ibiod.2020.104922.

[14] Stout, S.A., Wang, Z., 2007. Chemical fingerprinting of spilled or discharged petroleum: methods and factors affecting petroleum fingerprints in the environment. In: Wang, Z., Stout, S.A. (Eds.), Oil spill environmental forensics: fingerprinting and source identification. Academic Press, pp. 1–53. https://doi.org/10.1016/B978-012369523-9.50005-7.

[15] Kruge, M.A., Gallego, J.L.R., Lara-Gonzalo, A., Esquinas, N., 2018. Environmental forensics study of crude oil and petroleum product spills in coastal and oilfield settings: combined insights from conventional GC-MS, thermodesorption-GC-MS, and pyrolysis-GC-MS. In: Stout, S.A., Wang, Z. (Eds.), Oil spill environmental forensics case studies. Butterworth-Heinemann, pp. 131–155. https://doi.org/10.1016/B978-0-12-804434-6.00007-0.

[16] Kruge, M.A., Lara-Gonzalo, A., Gallego, J.L.R., 2020. Environmental forensics of complexly contaminated sites: a complimentary fingerprinting approach. Environ Pollut 263, 114645. https://doi.org/10.1016/j.envpol.2020.114645.

[17] Seeley, M.E., Lynch, J.M., 2023. Previous successes and untapped potential of pyrolysis-GC/MS for the analysis of plastic pollution. Anal Bioanal Chem 415 (15), 2873–2890. https://doi.org/10.1007/s00216-023-04671-1.

[18] Peláez, A.I., Lores, I., Sotres, A., Mendez-Garcia, C., Fernandez-Velarde, C., Santos, J.A., et al., 2013. Design and field-scale implementation of an 'on site' bioremediation treatment in PAH-polluted soil. Environ Pollut 181, 190–199. https://doi.org/10.1016/j.envpol.2013.06.004.

[19] Forján, R., Lores, I., Sierra, C., Baragaño, D., Gallego, J.L.R., Peláez, A.I., 2020. Bioaugmentation treatment of a PAH-polluted soil in a slurry bioreactor. Appl Sci 10 (8), 2837. https://doi.org/10.3390/app10082837.

[20] Gallego, J.L.R., Sierra, C., Permanyer, A., Peláez, A.I., Menéndez-Vega, D., Sánchez, J., 2011. Full-scale remediation of a jet fuel-contaminated soil: assessment of biodegradation, volatilization, and bioavailability. Water Air Soil Pollut 217 (1-4), 197–211. https://doi.org/10.1007/s11270-010-0579-6.

[21] Nikolopoulou, M., Kalogerakis, N., 2008. Enhanced bioremediation of crude oil utilizing lipophilic fertilizers combined with biosurfactants and molasses. Mar Pollut Bull 56 (11), 1855–1861. https://doi.org/10.1016/j.marpolbul.2008.07.021.

[22] Ortega, M.F., Guerrero, D.E., García-Martínez, M.J., Bolonio, D., Llamas, J.F., Canoira, L., et al., 2018. Optimization of landfarming amendments based on soil texture and crude oil concentration. Water Air Soil Pollut 229 (7), 234. https://doi.org/10.1007/s11270-018-3891-1.

[23] Gallego, J.L.R., Fernández, J.R., Díez-Sanz, F., Ordoñez, S., Sastre, H., González-Rojas, E., et al., 2007. Bioremediation for shoreline cleanup: In situ vs. on-site treatments. Environ Eng Sci 24 (4), 493–504. https://doi.org/10.1089/ees.2006.0091.

[24] Lara-Gonzalo, A., Kruge, M.A., Lores, I., Gutiérrez, B., Gallego, J.R., 2015. Pyrolysis GC-MS for the rapid environmental forensic screening of contaminated brownfield soil. Org Geochem 87, 9–20. https://doi.org/10.1016/j.orggeochem.2015.06.012.

[25] Kienhuis, P.A., Hansen, A.B., Fakness, L.G., Stout, S.A., Dahlmann, G., 2016. CEN methodology for oil spill identification. In: Stout, S.A., Wang, Z. (Eds.), Standard handbook oil spill environmental forensics. Academic Press, pp. 685–728. https://doi.org/10.1016/B978-0-12-803832-1.00014-3.

[26] Peña-Álvarez, V., Asensio, V., Baragaño, D., Forján, R., Peláez, A.I., Gallego, J.L.R., 2025. Integrated landfarming strategy for remediation of HCH-contaminated soil: synergistic effects of bioaugmentation, organic amendments, and nanoscale zero-valent iron. J Hazard Mater 489, 137637. https://doi.org/10.1016/j.jhazmat.2025.137637.

[27] Peña-Álvarez, V., Baragaño, D., Prosenkov, A., Gallego, J.R., Peláez, A.I., 2024. Assessment of co-contaminated soil amended by graphene oxide: effects on pollutants, microbial communities and soil health. Ecotoxicol Environ Saf 272, 116015. https://doi.org/10.1016/j.ecoenv.2024.116015.

[28] Wu, M., Guo, X., Wu, J., Chen, K., 2020. Effect of compost amendment and bioaugmentation on PAH degradation and microbial community shifting in petroleum-contaminated soil. Chemosphere 256, 126998. https://doi.org/10.1016/j.chemosphere.2020.126998.

[29] Kaplan, C.W., Kitts, C.L., 2004. Bacterial succession in a petroleum land treatment unit. Appl Environ Microbiol 70 (3), 1777–1786. https://doi.org/10.1128/AEM.70.3.1777-1786.2004.

[30] Jing, R., Fusi, S., Kjellerup, B.V., 2018. Remediation of polychlorinated biphenyls (PCBs) in contaminated soils and sediment: state of knowledge and perspectives. Front Environ Sci 6, 79. https://doi.org/10.3389/fenvs.2018.00079.

[31] Borja, J., Taleon, D.M., Auresenia, J., Gallardo, S., 2005. Polychlorinated biphenyls and their biodegradation. Process Biochem 40 (6), 1999–2013. https://doi.org/10.1016/j.procbio.2004.08.006.

[32] Abramowicz, D.A., 1990. Aerobic and anaerobic biodegradation of polychlorinated biphenyls: a review. Crit Rev Biotechnol 10 (3), 241–251. https://doi.org/10.3109/07388559009038210.

[33] Passatore, L., Rossetti, S., Juwarkar, A.A., Massacci, A., 2014. Phytoremediation and bioremediation of polychlorinated biphenyls (PCBs): state of knowledge and research perspectives. J Hazard Mater 278, 189–202. https://doi.org/10.1016/j.jhazmat.2014.05.051.

[34] Egene, C.E., Van Poucke, R., Ok, Y.S., Meers, E., Tack, F.M.G., 2018. Impact of organic amendments (biochar, compost and peat) on Cd and Zn mobility and solubility in contaminated soil of the Campine region after three years. Sci Total Environ 626, 195–202. https://doi.org/10.1016/j.scitotenv.2018.01.054.

[35] Houben, D., Evrard, L., Sonnet, P., 2013. Mobility, bioavailability and pH-dependent leaching of Cd, Zn and Pb in a contaminated soil amended with biochar. Chemosphere 92, 1450–1457. https://doi.org/10.1016/j.chemosphere.2013.03.055.

[36] Li, S., Sun, X., Li, S., Liu, Y., Ma, Q., Zhou, W., 2021. Effects of amendments on the bioavailability, transformation and accumulation of heavy metals by pakchoi cabbage in a multi-element contaminated soil. RSC Adv 11 (8), 4395–4405. https://doi.org/10.1039/d0ra09358k.

[37] Castaño, A., Prosenkov, A., Baragaño, D., Otaegui, N., Sastre, H., Rodríguez-Valdés, E., et al., 2021. Effects of in situ remediation with nanoscale zero valence iron on the physicochemical conditions and bacterial communities of groundwater contaminated with arsenic. Front Microbiol 12, 643589. https://doi.org/10.3389/fmicb.2021.643589.
[38] Catania, V., Bueno, R.S., Alduina, R., Grilli, E., La Mantia, T., Castaldi, S., et al., 2022. Soil microbial biomass and bacterial diversity in southern European regions vulnerable to desertification. Ecol Indic 145, 109725. https://doi.org/10.1016/j.ecolind.2022.109725.
[39] Frey, B., Moser, B., Tytgat, B., Zimmermann, S., Alberti, J., Biederman, L.A., et al., 2023. Long-term N-addition alters the community structure of functionally important N-cycling soil microorganisms across global grasslands. Soil Biol Biochem 176, 108887. https://doi.org/10.1016/j.soilbio.2022.108887.
[40] Widdig, M., Schleuss, P.M., Weig, A.R., Guhr, A., Biederman, L.A., Borer, E.T., et al., 2019. Nitrogen and phosphorus additions alter the abundance of phosphorus-solubilizing bacteria and phosphatase activity in grassland soils. Front Environ Sci 7, 185. https://doi.org/10.3389/fenvs.2019.00185.
[41] Zhou, J., Ma, M., Guan, D., Jiang, X., Zhang, N., Shu, F., et al., 2021. Nitrogen has a greater influence than phosphorus on the diazotrophic community in two successive crop seasons in Northeast China. Sci Rep 11 (1), 6303. https://doi.org/10.1038/s41598-021-85829-8.
[42] Ramadass, K., Megharaj, M., Venkateswarlu, K., Naidu, R., 2018. Bioavailability of weathered hydrocarbons in engine oil-contaminated soil: impact of bioaugmentation mediated by Pseudomonas spp. on bioremediation. Sci Total Environ 636, 968–974. https://doi.org/10.1016/j.scitotenv.2018.04.379.
[43] Daâssi, D., Qabil Almaghribi, F., 2022. Petroleum-contaminated soil: environmental occurrence and remediation strategies. 3 Biotech 12 (6), 139. https://doi.org/10.1007/s13205-022-03198-z.
[44] Ou, Y., Wu, M., Yu, Y., Liu, Z., Zhang, Y., Yi, N., 2024. Nitrogen utilization efficiency assessment during bioremediation of petroleum-contaminated loess soils: insights from metagenomic analysis. J Hazard Mater 478, 135506. https://doi.org/10.1016/j.jhazmat.2024.135506.
[45] Kundu, A., Harrisson, O., Ghoshal, S., 2022. Evaluating the impact of nutrient doses on biostimulation of petroleum hydrocarbon biodegradation in cold region soils. ACS ES&T Eng 2 (12), 2287–2300. https://doi.org/10.1021/acsestengg.2c00220.
[46] Gallego, J.R., Menéndez-Vega, D., González-Rojas, E., Sánchez, J., Garcia-Martínez, M.J., Llamas, J.F., 2006. Oleophilic fertilizers and bioremediation: a new perspective. In: Mendez-Vilas, A. (Ed.), Modern multidisciplinary applied microbiology: exploiting microbes and their interactions. Wiley-VCH, pp. 551–555. https://doi.org/10.1002/9783527611904.ch97.
[47] Jiménez, N., Viñas, M., Sabaté, J., Díez, S., Bayona, J.M., Solanas, A.M., et al., 2006. The Prestige oil spill. 2. Enhanced biodegradation of a heavy fuel oil under field conditions by the use of an oleophilic fertilizer. Environ Sci Technol 40 (8), 2578–2585. https://doi.org/10.1021/es052370z.
[48] Calvo, C., Silva-Castro, G.A., Uad, I., García Fandiño, C., Laguna, J., González-López, J., 2008. Efficiency of the EPS emulsifier produced by Ochrobactrum anthropi in different hydrocarbon bioremediation assays. J Ind Microbiol Biotechnol 35 (11), 1493–1501. https://doi.org/10.1007/s10295-008-0451-5.
[49] Kraut-Cohen, J., Zolti, A., Rotbart, N., Bar-Tal, A., Laor, Y., Medina, S., et al., 2023. Short- and long-term effects of continuous compost amendment on soil microbiome community. Comput Struct Biotechnol J 21, 3280–3292. https://doi.org/10.1016/j.csbj.2023.05.030.
[50] Luo, Y., van Veelen, H.P.J., Chen, S., Sechi, V., ter Heijne, A., Veeken, A., et al., 2022. Effects of sterilization and maturity of compost on soil bacterial and fungal communities and wheat growth. Geoderma 409, 115598. https://doi.org/10.1016/j.geoderma.2021.115598.
[51] Chiodi, C., Zardinoni, G., Stevanato, P., Giagnoni, L., Carletti, P., Oustrière, N., et al., 2025. Organic amendments influence soil properties, soil microbial diversity, and winter barley traits in a five-year field trial with contaminated soils at a former wood preservation site. Chem Biol Technol Agric 12 (1), 87. https://doi.org/10.1186/s40538-025-00810-1.
[52] Farrell, M., Griffith, G.W., Hobbs, P.J., Perkins, W.T., Jones, D.L., 2009. Microbial diversity and activity are increased by compost amendment of metal-contaminated soil. FEMS Microbiol Ecol 71 (1), 94–105. https://doi.org/10.1111/j.1574-6941.2009.00793.x.
[53] Wallisch, S., Gril, T., Dong, X., Welzl, G., Bruns, C., Heath, E., et al., 2014. Effects of different compost amendments on the abundance and composition of alkB-harboring bacterial communities in a soil under industrial use contaminated with hydrocarbons. Front Microbiol 5, 96. https://doi.org/10.3389/fmicb.2014.00096.
[54] Gao, J., Han, H., Gao, C., Wang, Y., Dong, B., Xu, Z., 2023. Organic amendments for in situ immobilization of heavy metals in soil: a review. Chemosphere 335, 139088. https://doi.org/10.1016/j.chemosphere.2023.139088.
[55] Tang, J., Zhang, L., Zhang, J., Ren, L., Zhou, Y., Zheng, Y., et al., 2020. Physicochemical features, metal availability and enzyme activity in heavy metal-polluted soil remediated by biochar and compost. Sci Total Environ 701, 134751. https://doi.org/10.1016/j.scitotenv.2019.134751.
[56] Esquinas, N., Rodríguez-Valdés, E., Márquez, G., Gallego, J.L.R., 2017. Diagnostic ratios for the rapid evaluation of natural attenuation of heavy fuel oil pollution along shores. Chemosphere 184, 1089–1098. https://doi.org/10.1016/j.chemosphere.2017.06.087.
[57] Fritt-Rasmussen, J., Wegeberg, S., Gustavson, K., Sørheim, K.R., Daling, P.S., Jørgensen, K., (2018). Heavy fuel oil (HFO): a review of fate and behaviour of HFO spills in cold seawater, including biodegradation, environmental effects and oil spill response. Nordic Council of Ministers. [TemaNord 2018:549]. https://doi.org/10.6027/TN2018-549.
[58] Gros, J., Reddy, C.M., Aeppli, C., Nelson, R.K., Carmichael, C.A., Arey, J.S., 2014. Resolving biodegradation patterns of persistent saturated hydrocarbons in weathered oil samples from the deepwater horizon disaster. Environ Sci & Technol 48 (3), 1628–1637. https://doi.org/10.1021/es4042836.
[59] Peters, K.E., Walters, C.C., Moldowan, J.M., 2005. The biomarker guide (Vol. 2, 2nd ed.): biomarkers and isotopes in petroleum systems and earth history. Cambridge University Press. https://doi.org/10.1017/CBO9781107326040.
[60] Wang, Z., Fingas, M.F., 2003. Development of oil hydrocarbon fingerprinting and identification techniques. Mar Pollut Bull 47 (9), 423–452. https://doi.org/10.1016/S0025-326X(03)00215-7.
[61] Aeppli, C., Nelson, R.K., Radović, J.R., Carmichael, C.A., Valentine, D.L., Reddy, C.M., 2014. Recalcitrance and degradation of petroleum biomarkers upon abiotic and biotic natural weathering of deepwater horizon oil. Environ Sci Technol 48 (12), 6726–6734. https://doi.org/10.1021/es500825q.
[62] Ma, X., Shang, P., Mei, Z., Lu, Z., Gong, Y., Zhang, H., et al., 2025. Environmental safety perspectives on organophosphate flame retardants: current strategies and advancements in their environmental removal and detection. J Environ Chem Eng 13, 115340. https://doi.org/10.1016/j.jece.2025.115340.
[63] Thuy, T.L., Hoang, T.-D., Hoang, V.-H., Nguyen, M.-K., 2025. A review on flame retardants in soils: occurrence, environmental impact, health risks, remediation strategies, and future perspectives. Toxics 13 (3), 228. https://doi.org/10.3390/toxics13030228.
[64] Van den Eede, N., Tomy, G., Tao, F., Halldorson, T., Harrad, S., Neels, H., et al., 2016. Kinetics of tris (1-chloro-2-propyl) phosphate (TCIPP) metabolism in human liver microsomes and serum. Chemosphere 144, 1299–1305. https://doi.org/10.1016/j.chemosphere.2015.09.049.
[65] Paluselli, A., Fauvelle, V., Galgani, F., Sempéré, R., 2019. Phthalate release from plastic fragments and degradation in seawater. Environ Sci Technol 53 (1), 166–175. https://doi.org/10.1021/acs.est.8b05083.
[66] Zhang, H., Che, T., Yu, H., Yue, J., Wang, Q., 2026. Phthalate ester pollution poses a potential threat to soil organisms: Insights from a global meta and machine-learning analysis. Environ Res 290, 123467. https://doi.org/10.1016/j.envres.2025.123467.
[67] Puglisi, E., Nicelli, M., Capri, E., Trevisan, M., Del Re, A.A., 2003. Cholesterol, beta-sitosterol, ergosterol, and coprostanol in agricultural soils. J Environ Qual 32 (2), 466–471. https://doi.org/10.2134/jeq2003.4660.
[68] Bataglion, G.A., Koolen, H.H., Weber, R.R., Eberlin, M.N., 2016. Quantification of sterol and triterpenol biomarkers in sediments of the Cananéia-Iguape estuarine-lagoonal system (Brazil) by UHPLC-MS/MS. Int J Anal Chem 2016, 8361375. https://doi.org/10.1155/2016/8361375.
[69] Barakat, A.O., Qian, Y., Kim, M., Kennicutt II, M.C., 2001. Chemical characterization of naturally weathered oil residues in arid terrestrial environment in Al-Alamein, Egypt. Environ Int 27 (4), 291–310. https://doi.org/10.1016/S0160-4120(01)00060-5.
[70] Yang, Z., Hua, Y., Mirnaghi, F., Hollebone, B.P., Jackman, P., Brown, C.E., et al., 2018. Effect of evaporative weathering and oil-sediment interaction on the fate and behavior of diluted bitumen in marine environments. Part 2. The water accommodated and particle-laden hydrocarbon species and toxicity of the aqueous phase. Chemosphere 191, 145–155. https://doi.org/10.1016/j.chemosphere.2017.10.033.
[71] Oudot, J., Chaillan, F., 2010. Pyrolysis of asphaltenes and biomarkers for the fingerprinting of the Amoco-Cadiz oil spill after 23 years. Comptes Rendus Chim 13 (5), 548–552. https://doi.org/10.1016/j.crci.2009.12.002.
[72] Romero-Silva, R., Zafra, G., Quintero, J.C., 2019. Bioremediation of soils contaminated with petroleum solid wastes and asphaltenes using native microbial consortia. SN Appl Sci 1, 1209. https://doi.org/10.1007/s42452-019-1236-3.
[73] Liu, L., Liu, C., Fu, R., Nie, F., Zuo, W., Tian, Y., et al., 2024. Full-chain analysis on emerging contaminants in soil: source, migration and remediation. Chemosphere 363, 142854. https://doi.org/10.1016/j.chemosphere.2024.142854.
[74] Picó, Y., Barceló, D., 2020. Pyrolysis gas chromatography-mass spectrometry in environmental analysis: focus on organic matter and microplastics. TrAC Trends Anal Chem 130, 115964. https://doi.org/10.1016/j.trac.2020.115964.